mouse spleen endothelial line MSS31 were cultured in αMEM (Sigma) supplemented with 10% fetal bovine serum (FBS) [20,21]. NIH 3T3 cells and MC3T3-E1 cells were maintained in DMEM (Sigma) or αMEM supplemented with 10% FBS. ATDC5 cells were cultured in a 1:1 mixture of DMEM and Ham's F-12 medium supplemented with 5% FBS, 10 μg/ml human insulin (Roche, Mannheim, Germany), 10 μg/ml human transferrin (Roche), and 3×10^{-8} M sodium selenite (Sigma), as previously described [22]. Cell cultures were performed at 37 °C in a humidified incubator with 5% CO_2.

Tube formation, cell adhesion, and cell migration assay

Bioassays were performed as previously described with some modifications [18]. Briefly, in each assay, cells were serum-starved for 4 h in αMEM containing 0.5% FBS and harvested. For tube formation assay, serum-starved HUVECs were resuspended in αMEM containing 0.1% BSA (4×10^4 cells/500 μl) and preincubated with reagents for 30 min at 37 °C. The cells were then plated on growth factor-reduced Matrigel (BD Biosciences, Bedford, MA) diluted 1:1 with serum-free αMEM in 24-well cell culture plates and allowed to form tube-like structures for 6 h in the presence of VEGF-A (20 ng/ml). The tube-like cellular networks were fixed and measured using IPLab Scientific Imaging Software (Scanalytic Inc., Fairfax, VA). For cell adhesion assays, 96-multiwell plates were coated with type I collagen (50 μg/ml; Koken, Tokyo, Japan), fibronectin (10 μg/ml; BD Biosciences), or vitronectin (5 μg/ml; BD Biosciences) at 4 °C overnight and blocked with 2% BSA/PBS for 30 min at 37 °C. Coated wells were then washed twice with PBS. HUVECs (5×10^4 cells in 100 μl of αMEM containing 0.5% BSA) were allowed to adhere for 30 min at 37 °C. Cell adhesion was determined by measuring the absorbance of crystal violet-stained cells at 595 nm. For cell migration assay, cell culture inserts (8 μm pore size; BD Biosciences) were coated with 1–2 μg/ml vitronectin at 4 °C overnight. The cells were resuspended in αMEM containing 0.1% BSA (7×10^4 cells/200 μl), preincubated with reagents for 30 min, and then allowed to migrate for 4 h at 37 °C in the same medium containing VEGF-A, FGF-2, or other chemotactic stimulators that had been added to the lower chamber in the presence or absence of inhibiting reagents. The number of cells that had migrated to the bottom surface of the insert was counted in five representative high power fields (200× magnification) per insert.

RNA preparation and RT-PCR

Total RNA was prepared from cells grown to subconfluence using the single-step method of Chomczynski and Sacchi [23]. First strand cDNA was synthesized from 1 μg of total RNA using SuperScript II RNase H^- reverse transcriptase (Gibco BRL, Grand Island, NY). The primer sequences used for RT-PCR analyses were as follows: glyceraldehyde-3-phosphate-dehydrogenase (GAPDH) forward primer: 5′-ACCACAGTCCATGCCATCAC-3′; GAPDH reverse primer: 5′-TCCACCACCCTGTTGCTGTA-3′; mouse VEGF receptor-2 (VEGFR-2) forward primer: 5′-CACAGACACCACCGTGTACTCC-3′; mouse VEGFR-2 reverse primer: 5′-CTCCAAGGTAGACAGACTCGGC-3′; human VEGFR-2 forward primer: 5′-GTGACCAACATGGAGTCGTG-3′; human VEGFR-2 reverse primer: 5′-CCAGAGATTCCATGCCACTT-3′; bovine VEGFR-2 forward primer: 5′-CACGGACACCACTGTGTACTCC-3′; bovine VEGFR-2 reverse primer: 5′-ACCTAAAGCACTTCCATTGTCTG-3′; mouse FGF receptor-1 (FGFR-1) forward primer: 5′-AGAGACCAGCTGTGATGA-3′; mouse FGFR-1 reverse primer: 5′-GGCCACTTTGGTCACACG-3′; human FGFR-1 forward primer: 5′-GGAGGATCGAGCTCACTCGTGG-3′; human FGFR-1 reverse primer: 5′-CGGAGAAGTAGGTGGTGTCAC-3′; bovine FGFR-1 forward primer: 5′-AGAGACCGGCGGTGATGA-3′; bovine FGFR-1 reverse primer: 5′-GGCCACTTTGGTCACACG-3′. GAPDH amplification was utilized as an internal control and the primer pairs were designed using the consensus sequences between the mouse and human versions of this gene.

Immunoblotting

For the adhesion-dependent FAK activation, HUVECs were harvested and resuspended in serum-free medium containing 0.1% BSA. The cells were kept in suspension for 30 min at 37 °C with or without rhChM-I (1.5 μg/ml) and then plated on the vitronectin-coated plates. Cells were allowed to adhere for the indicated time and lysed with SDS sample buffer [50 mM Tris–HCl (pH6.8), 2% SDS, 50 mM dithiothreitol (DTT), and 10% glycerol], boiled for 5 min, and subjected to immunoblotting analysis. Samples were separated by SDS–polyacrylamide gel electrophoresis (SDS–PAGE) and transferred onto nitrocellulose membrane (Bio-Rad, Hercules, CA). Blotted membranes were preincubated with 3.2% skim milk in Tris-buffered saline [TBS; 20 mM Tris, pH 7.4, 150 mM NaCl] for 30 min and incubated with primary antibody at 4 °C overnight. Blots were washed with TBS containing 0.05% Tween 20 and incubated with horseradish peroxidase-conjugated anti-mouse IgG antibody (GE Healthcare Bio-Sciences, Uppsala, Sweden). Detection of antibodies was performed using the ECL Western Blotting Detection Reagents (GE Healthcare Bio-Sciences).

Rac1/Cdc42 pull-down assay

Subconfluent HUVECs were serum-starved for 4 h in αMEM containing 0.5% FBS, harvested, and resuspended in αMEM containing 0.1% BSA. The cells (1.5×10^6 cells) were preincubated with or without rhChM-I (1.5 μg/ml) for 1 h and then allowed to spread on vitronectin-coated 60-mm dishes for 30 min at 37 °C. For the VEGF-A-induced activation of Rac1 and Cdc42, subconfluent HUVECs were serum-starved for 4 h in αMEM containing 0.5% FBS and preincubated with or without rhChM-I (1 μg/ml) for 30 min. The cells were then stimulated with VEGF-A (20 ng/ml) for 30 min (Rac1) or 10 min (Cdc42). Cells were lysed in ice-cold lysis buffer containing 1% Triton X-100, 0.5% sodium deoxycholate, 0.1% SDS, 50 mM Tris–HCl (pH7.5), 500 mM NaCl, 10 mM $MgCl_2$, 1 μg/ml leupeptin, 1 μg/ml pepstatin, and 1 mM PMSF. Lysates were clarified by centrifugation and incubated with 20 μg of PAK-GST protein beads (Cytoskeleton Inc., Denver, CO) for 3 h at 4 °C. The beads were washed three times with the buffer containing 0.1% Triton X-100, 50 mM Tris–HCl (pH7.5), 150 mM NaCl, 5 mM $MgCl_2$, 10% glycerol, 1 μg/ml leupeptin, 1 μg/ml pepstatin, and 1 mM PMSF. Bound proteins were eluted by boiling in 20 μl of 2× SDS sample buffer and subjected to the immunoblot analysis with anti-Rac1 or anti-Cdc42 antibody. The relative activities of Rac1 and Cdc42 were determined by measuring the intensity of GTP-Rac1 and GTP-Cdc42 immunoreactivity normalized to that of total Rac1 or Cdc42 in whole cell lysates. These measurements

were made using Fuji Film Science Lab 99 Image Gauge ver. 3.4 software (Fuji Photo Film, Tokyo, Japan).

Immunofluorescence

HUVECs (1×10^4 cells) were cultured overnight on 8-well Lab-Tek II CC2 chamber slides (Nalgen Nunc International Corp, Naperville, IL) coated with vitronectin, and serum-starved for 5 h in αMEM containing 0.5% FBS. The cells were then incubated with 0.1% BSA/PBS or rhChM-I for 30 min at 37 °C prior to the addition of VEGF-A (25 ng/ml). After 1 h of further culture, the cells were fixed with 4% PFA/PBS, permeabilized with 0.2% Triton X-100 for 4 min, and incubated with 5% skim milk/PBS for 20 min. These preparations were then incubated with anti-paxillin mAb at 4 °C overnight followed by 1 h incubation with Alexa Fluor 594-conjugated phalloidin, Alexa Fluor 488-conjugated goat anti-mouse IgG secondary antibody, and 1 μg/ml of 4′, 6-diamidino-2-phenylindole (DAPI, Sigma) in 5% skim milk/PBS. Slides were observed under a fluorescence microscope (Leica Microsystems, Mannheim, Germany).

Time-lapse analysis

Serum-starved HUVECs were plated on vitronectin-coated dishes and allowed to adhere for 1 h at 37 °C in αMEM containing 0.5% FBS. The cells were preincubated with or without rhChM-I for 30 min and then stimulated with VEGF-A (25 ng/ml). The cells were observed under a microscope (DM IRBE, Leica Microsystems) at 37 °C in a CO_2 incubation system (Tokken, Chiba, Japan). Time-lapse images were recorded at 2-min intervals for 4 h (120 frames) with a digital CCD camera (Hamamatsu, Shizuoka, Japan). Images were automatically collected and quantified using IPLab Scientific Imaging Software (Scanalytic Inc., Fairfax, VA). The frequency and persistence of cell protrusions were analyzed at 120–180 min after the addition of VEGF-A and were calculated as the average number of protrusions per cell and the average extending time of protrusion per cell during the observations, respectively. Cell migration was analyzed manually by marking the position of the nucleus in individual cells in selected frames (i.e. at 30-min intervals) to obtain migration tracks. The migration speed was determined as the total migration distance (T) divided by the total migration time (4 h). Net translocation distance (D) was calculated as a linear distance between the initial point and the end point of the observation. The directionality of cell migration was calculated as a D/T ratio. Four independent experiments were carried out and the migration tracks of 15–30 cells were extracted from each experiment to obtain at least the migration tracks of 75 cells to be analyzed.

Results

Anti-angiogenic activity of rhChM-I prepared from serum-free culture of 293-F cells

Recombinant human ChM-I (rhChM-I) was expressed with an N-terminal FLAG tag in a serum-free culture of 293-F cells and purified using anti-FLAG M2 affinity gel. The bioactivity of rhChM-I was confirmed via a tube formation assay of HUVECs cultured on Matrigel (Table 1). The inhibitory effects of rhChM-I were comparable to that of our previous preparation from CHO cells (CHO-hChM-I, 1 μg/ml) with a reduction-oxidation procedure [9], and more potent than that of endostatin (3 μg/ml), a cryptic angiogenesis inhibitor derived from type XVIII collagen [24]. We then examined the anti-angiogenic activity of rhChM-I *in vivo* using a mouse corneal micropocket assay (Fig. 1). At day 14 after implantation of HEME pellets, VEGF-A (160 ng/pellet) induced the growth of new blood vessels (CD31-positive) and also lymphatic vessels (CD31 and LYVE1 double-positive) sprouting from the corneal limbus (Figs. 1D–F). In contrast, application of VEGF-A together with rhChM-I (34 ng/pellet) led to an efficient suppression of newly formed blood vessels and lymphatic vessels (Fig. 1G–I, J, and K). Thus, this preparation of rhChM-I was found to be biologically active both *in vitro* and *in vivo*. Without VEGF-A, application of rhChM-I alone had no significant effects on blood vessels and lymphatic vessels in mouse cornea (Fig. S1).

Table 1 – Effects of recombinant human ChM-I on the tube morphogenesis of HUVECs.

Additions[a]	Tube length (mm)/field[b]
0.1% BSA/PBS alone	2.86 ± 0.73
0.1% BSA/PBS+ VEGF-A	9.20 ± 1.14
CHO-hChM-I+ VEGF-A	5.21 ± 0.64
rhChM-I+ VEGF-A	4.89 ± 0.94
Endostatin+ VEGF-A	7.36 ± 1.59

[a] HUVECs were suspended in serum-free medium and incubated with 0.1% BSA/PBS, CHO-hChM-I (1 μg/ml), rhChM-I (1 μg/ml), or endostatin (3 μg/ml) for 30 min, respectively.

[b] The cells were plated onto growth factor-reduced Matrigel in the presence or absence of VEGF-A (20 ng/ml). Tube-like structures were allowed to form for 6 h, fixed, and then photographed. The total tube length per field was measured using image processing and analysis software. The data shown are the average of five fields. Similar results were obtained from two independent experiments.

Inhibition of VEGF-A-induced migration of HUVECs by rhChM-I and its selective actions

Cell migration is one of the critical steps during angiogenesis, and is therefore a common target of many angiogenesis inhibitors such as endostatin, angiostatin, and arresten [16,25]. We evaluated the effects of rhChM-I on cell migration using a modified Boyden chamber assay (Fig. 2). Serum-starved HUVECs were seeded onto the upper chamber and chemotactic migration was induced by the addition of VEGF-A (20 ng/ml) in the lower chamber. Upon treatment with VEGF-A, cell migration was induced 3- to 4-fold above the basal level on the vitronectin-coated surface. Endostatin successfully inhibited this VEGF-A-induced migration, as previously reported [24,26]. Recombinant hChM-I did not affect the basal levels of migration, but significantly inhibited the VEGF-A-induced migration in a dose dependent manner. The concentration required for 50% inhibition (ID_{50}) in this experiment was measured at 83 ng/ml. Similarly, the inhibitory action of rhChM-I was also observed in the VEGF-A-induced 3D cell migration of HUVECs through Matrigel matrix (Fig. S2). Although rhChM-I inhibited the VEGF-A-induced migration without affecting the basal level of migration in

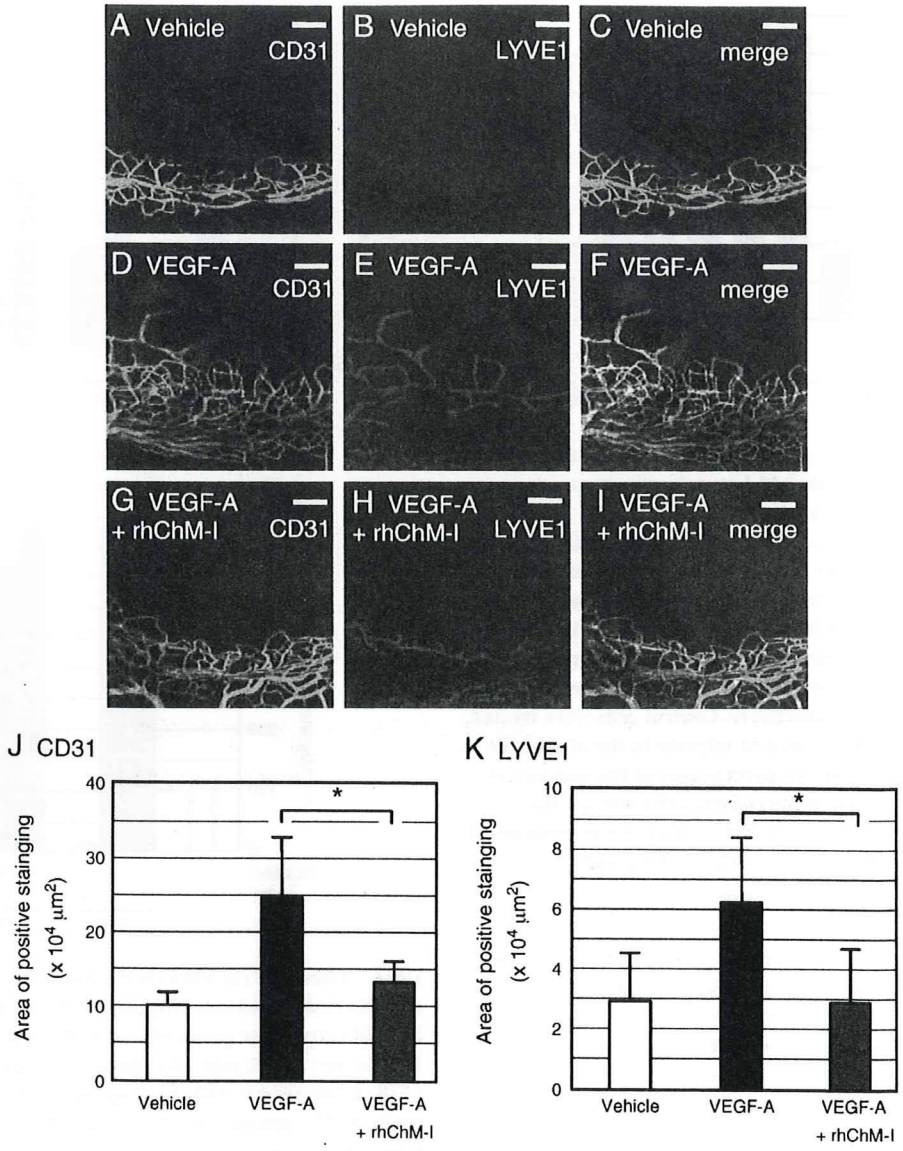

Fig. 1 – Effects of rhChM-I on VEGF-A-induced corneal angiogenesis and lymphangiogenesis. (A–I) HEME pellets containing either vehicle (A–C) or VEGF-A (160 ng) (D–I) were implanted into the micropocket of the mouse cornea with (G–I) or without (A–F) rhChM-I (34 ng/pellet). At day 14 after implantation, corneal tissues were excised and subjected to the whole-mount double immunostaining with antibodies against CD31 (*green*; A, D, and G) and LYVE1 (*red*; B, E, and H). Merged images were shown in panels C, F, and I. Bars, 200 μm. (J–K) Images of CD31-positive (J) and LYVE1-positive (K) staining area were captured in five different fields for each animal and quantified as described in Materials and methods. Values are the means ± SD from five animals/group. *$P < 0.05$.

HUVECs, the signal entry from VEGFR-2 and the downstream signaling of ERK1/2, c-Src, and focal adhesion kinase (FAK) were not affected by rhChM-I (Figs. S3A–C).

Various growth factors and agents are known to induce the chemotactic migration of vascular endothelial cells. Similar to VEGF-A (20 ng/ml), FGF-2 (20 ng/ml) and IGF-I (50 ng/ml) were both found to be capable of inducing the migration of HUVECs (Fig. 3A). The maximal dose of rhChM-I (1.5 μg/ml) inhibited 78% of the VEGF-A-induced migration of cells. Similarly, rhChM-I inhibited 71% and 78% of the FGF-2-induced and IGF-I-induced migration of HUVECs, respectively (Fig. 3A). In contrast, rhChM-I had little impact upon the effects of PMA (phorbol 12-myristate 13-acetate) (3 nM), a protein kinase C (PKC) activator [27]. Furthermore, rhChM-I showed only a marginal effect on the HUVEC migration induced by 60 nM S1P (sphingosine 1-phosphate) (Fig. 3B), which among serum components has been reported to be a potent stimulator of cell migration [28]. As S1P acts through G protein-coupled

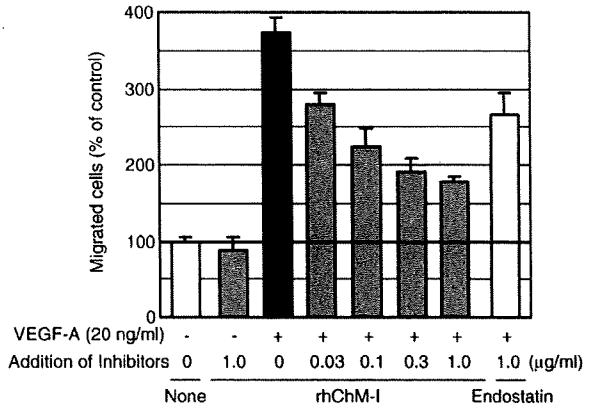

Fig. 2 – Effects of rhChM-I on the VEGF-A-induced migration of HUVECs. The effects of rhChM-I on cell migration were examined using a modified Boyden chamber assay. Serum-starved HUVECs (7×10^4 cells) were preincubated with angiogenesis inhibitors for 30 min, and then seeded onto vitronectin-coated cell culture inserts in serum-free medium. Chemotactic migration of HUVECs was induced by the addition of VEGF-A (20 ng/ml) in the lower chamber. Cells were allowed to migrate for 4 h in the presence of various concentrations of rhChM-I or endostatin, respectively. Control cells were treated with 0.1% BSA/PBS and allowed to migrate in the absence of VEGF-A. The values shown are percentages of the number of migrated cells compared to the control cells and are the means ± SD of a triplicate assay. The data are representative of three independent experiments with similar results.

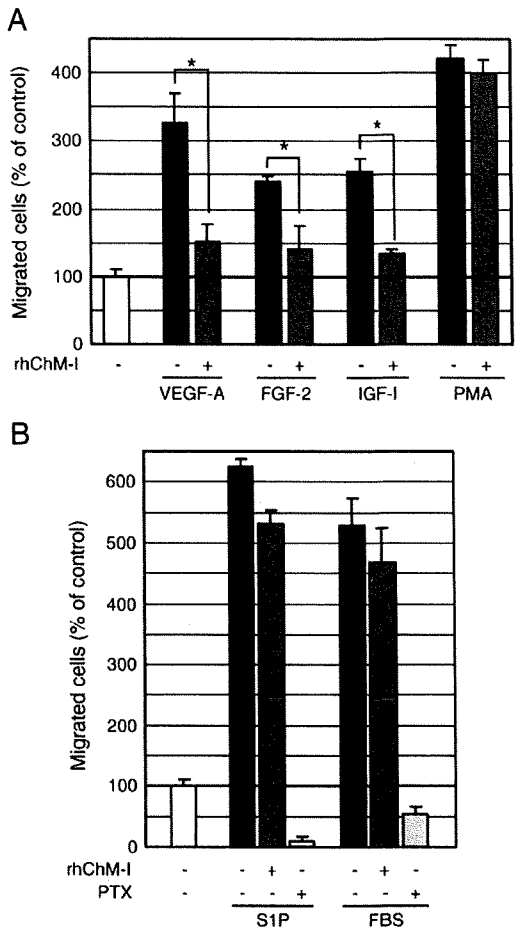

Fig. 3 – Effects of rhChM-I on the chemotactic migration of HUVECs toward various stimulants. (A) Serum-starved HUVECs (7×10^4 cells) were preincubated with or without rhChM-I (1.5 μg/ml) for 30 min and allowed to migrate for 4 h toward VEGF-A (20 ng/ml), FGF-2 (20 ng/ml), IGF-I (50 ng/ml), and PMA (3 nM), respectively. Values are the means ± SD of triplicate assays and the data are representative of three independent experiments. *$P<0.05$. (B) HUVECs were serum-starved for 4 h in the presence or absence of 100 ng/ml PTX. The cells were harvested and incubated with or without rhChM-I (1.5 μg/ml) for 30 min and then allowed to migrate for 4 h toward αMEM containing 2% FBS or S1P (60 nM). Values are the means ± SD of a triplicate assay. These data are representative of three independent experiments with similar results.

receptors (GPCRs) [29], a Gi-specific inhibitor, PTX, profoundly abrogated the motile property of HUVECs toward S1P. In addition, serum-induced HUVEC migration was also found to be Gi-dependent and insensitive to the inhibitory action of rhChM-I. These results suggest that ChM-I may affect the receptor tyrosine kinase (RTK) signals activated by the angiogenic growth factors.

FGF-2 stimulates the migration of a wide variety of mesenchymal cells through its RTK signaling pathway [30]. As expected from the abundant expression of FGF receptor-1 (FGFR-1) in NIH 3T3, chondrogenic ATDC5, and osteoblastic MC3T3-E1 cells (Fig. 4A), FGF-2 markedly stimulated the migration of these three cell types (Fig. 4C). However, rhChM-I exhibited no significant effects upon the migration of these fibroblastic cells, while synthetic inhibitor of the tyrosine kinase activity of FGFR-1, SU5040, completely blocked the FGF-2-induced migration of cells. In clear contrast, exposure to rhChM-I significantly inhibited the FGF-2-induced migration of both HUVECs and bovine aortic endothelial cells (BAECs). We also tested the migration of MSS31, a clonal cell line established from mouse spleen stroma. This cell line has been shown to exhibit the properties of endothelial cells; they express marker genes of vascular endothelial cells including VEGFR-1, VEGFR-2, and PECAM-1 and are able to form capillary-like structures in collagen matrices [20,21]. Treatment of MSS31 cells with rhChM-I completely blocked the FGF-2-induced migration (Fig. 4B). These results indicate that the inhibitory action of ChM-I is selective for vascular endothelial cell types.

Effects of rhChM-I on the cell adhesion and spreading of HUVECs

To examine the effects of rhChM-I on cell–matrix interactions, HUVECs treated with rhChM-I were plated onto bare plastic culture plates or culture plates coated with ECM proteins including type I collagen, fibronectin, or vitronectin for 30 min (Fig. 5A). Recombinant human ChM-I had no significant effects on the adhesion of HUVECs to either substrate. Non-specific cell adhesion to the bare plastic surface was not observed, because the cells

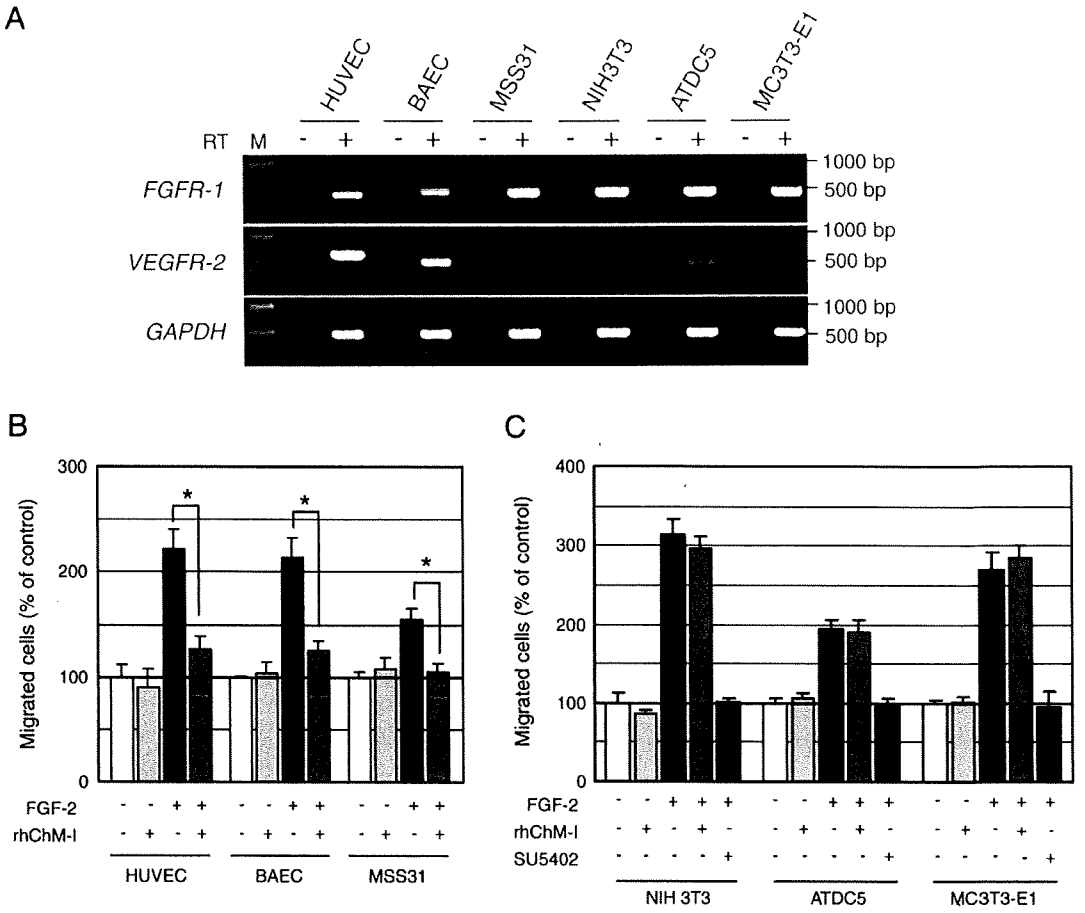

Fig. 4 – Effects of rhChM-I upon the FGF-2-induced migration of endothelial and non-endothelial cells. (A) RT-PCR analysis of VEGFR-2 and FGFR-1 expression in HUVECs, BAECs, MSS31, NIH 3T3, ATDC5, and MC3T3-E1 cells. The primer pairs used were designed to specifically amplify mouse VEGFR-2 (519 base pairs) and mouse FGFR-1 (461 base pairs) in MSS31, NIH 3T3, ATDC5, and MC3T3-E1 cells, human VEGFR-2 (600 base pairs) and human FGFR-1 (421 base pairs) in HUVECs, and bovine VEGFR-2 (497 base pairs) and bovine FGFR-1 (427 base pairs) in BAECs. GAPDH was used as an internal control. (B and C) FGF-2-induced migration of endothelial cells (B) and non-endothelial cells (C). Serum-starved cells (7×10^4 cells) were preincubated with or without rhChM-I (0.5 μg/ml) or SU5402 (20 μM) for 30 min and allowed to migrate for 4 h toward FGF-2 (20 ng/ml) in the presence or absence of inhibitors. Values are the means ± SD of a triplicate assay. The data are representative of three independent experiments. *$P<0.05$.

rarely adhered to the plastic surface under the experimental conditions. Consistent with these observations, treatment with rhChM-I resulted in no significant change upon the adhesion-dependent phosphorylation of FAK (pY397) in HUVECs, which is an indicator of activated FAK (Fig. 5B) [31]. Furthermore, rhChM-I additively inhibited the VEGF-A-induced migration of HUVECs in combination with the maximal dose of function-blocking antibody against integrin α5β1, a fibronectin receptor, and integrin αvβ3, a vitronectin receptor, indicating that the inhibitory action of rhChM-I is independent of the cell adhesion mediated by integrins (Fig. S4). However, rhChM-I caused a slight delay in cell spreading during the first 1 h after plating on vitronectin. Cells treated with rhChM-I displayed several spiky protrusions around the cell periphery, while control cells exhibited round morphologies (Fig. 5C). The number of cells with broad lamellipodia was considerably decreased during the first 1 h but recovered at 2 h after plating (Fig. 5D). As it has been shown that cell spreading proceeds with a reorganization of the actin cytoskeleton, we then assessed the activity of the Rho family small GTPases, Rac1 and Cdc42, which are key regulators of actin filaments and focal adhesion organization [32]. When rhChM-I-treated HUVECs were allowed to spread for 30 min on a vitronectin-coated surface, both of these activities were significantly suppressed (active Rac1, 55.6 ± 20.8% of control; active Cdc42, 41.3 ± 9.5% of control; Figs. 5E and F).

Effects of rhChM-I on the VEGF-A-induced actin cytoskeletal reorganization of HUVECs

As well as the cell–matrix interactions, VEGF-A is also known to stimulate the reorganization of the actin cytoskeleton, which underpins the effective migration of endothelial cells [33]. To investigate whether the action of rhChM-I is associated with this process, serum-starved HUVECs were stimulated by VEGF-A for 1 h and the actin filaments and focal adhesions were visualized by fluorescently labeled phalloidin and immunostaining using

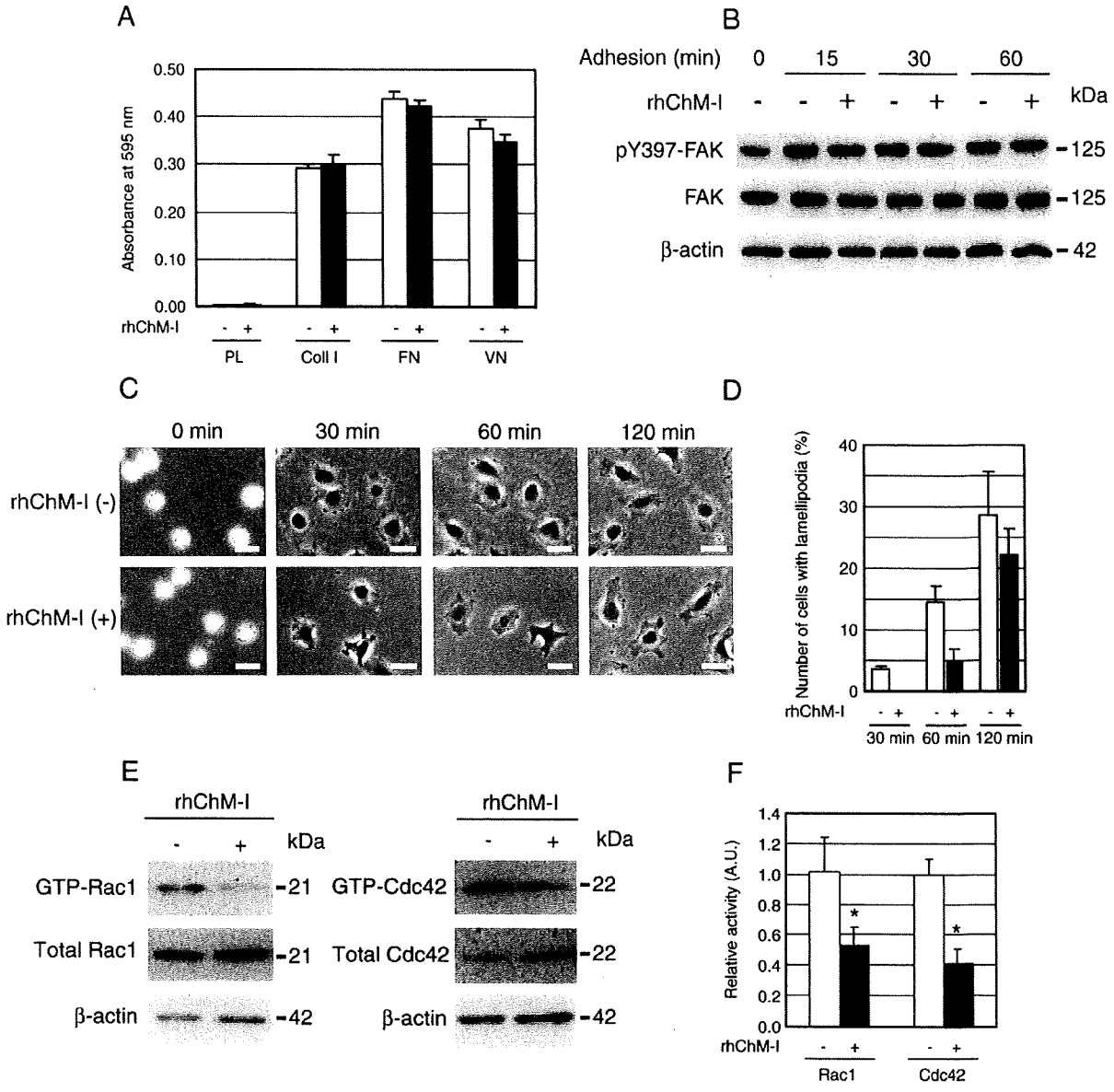

Fig. 5 – Effects of rhChM-I on the adhesion and spreading of HUVECs. (A) Adhesion of HUVECs to type I collagen-, fibronectin-, or vitronectin-coated culture plates or bare plastic culture plates. HUVECs were preincubated with or without rhChM-I (1.5 μg/ml) for 30 min before plating in non-coated plastic wells (PL) or wells coated with type I collagen (Col I, 50 μg/ml), fibronectin (FN, 10 μg/ml), and vitronectin (VN, 5 μg/ml), respectively. The cells were then allowed to adhere for 30 min. Non-adherent cells were removed by washing with PBS and the level of adhesion was determined by measuring the absorbance at 595 nm of crystal violet-stained cells. Values are the means ± SD of a triplicate assay and the data are the representative of three independent experiments with similar results. (B) Adhesion-dependent FAK activation in the absence or presence of rhChM-I. Serum-starved HUVECs were harvested and preincubated with or without rhChM-I (1.5 μg/ml) for 30 min and then allowed to adhere on vitronectin-coated plates. The adhered cells were lysed at the indicated times and the adhesion-dependent activation of FAK was evaluated using an anti-phospho-FAK (pY397) antibody. Equal loading of the samples was verified by an anti-β-actin antibody. (C and D) Spreading of HUVECs on vitronectin-coated plates. Serum-starved HUVECs were harvested and preincubated with or without rhChM-I (1.5 μg/ml) for 20 min prior to seeding onto vitronectin-coated plates. After plating, cell morphologies were captured at the indicated times using phase-contrast microscopy (C). The number of cells with lamellipodia was then counted (D). Values are the means ± SD of at least 200 randomly selected cells obtained in different fields from three independent experiments. Bars, 30 μm. (E and F) Cells were allowed to spread on vitronectin-coated dishes for 30 min in the presence or absence of rhChM-I (1.5 μg/ml) and lysed. Cell extracts were then affinity precipitated with PAK-GST protein beads and subjected to immunoblotting analysis to detect GTP-bound Rac1 (GTP-Rac1) and GTP-bound Cdc42 (GTP-Cdc42). Equal loading of the samples was verified by an anti-β-actin antibody (E). Levels of active Rac1 or Cdc42 were measured by densitometric analysis of immunoblots and normalized to the total levels of Rac1 or Cdc42 in the cell lysates (F). Values are the means ± SD from three independent experiments. *$P < 0.05$.

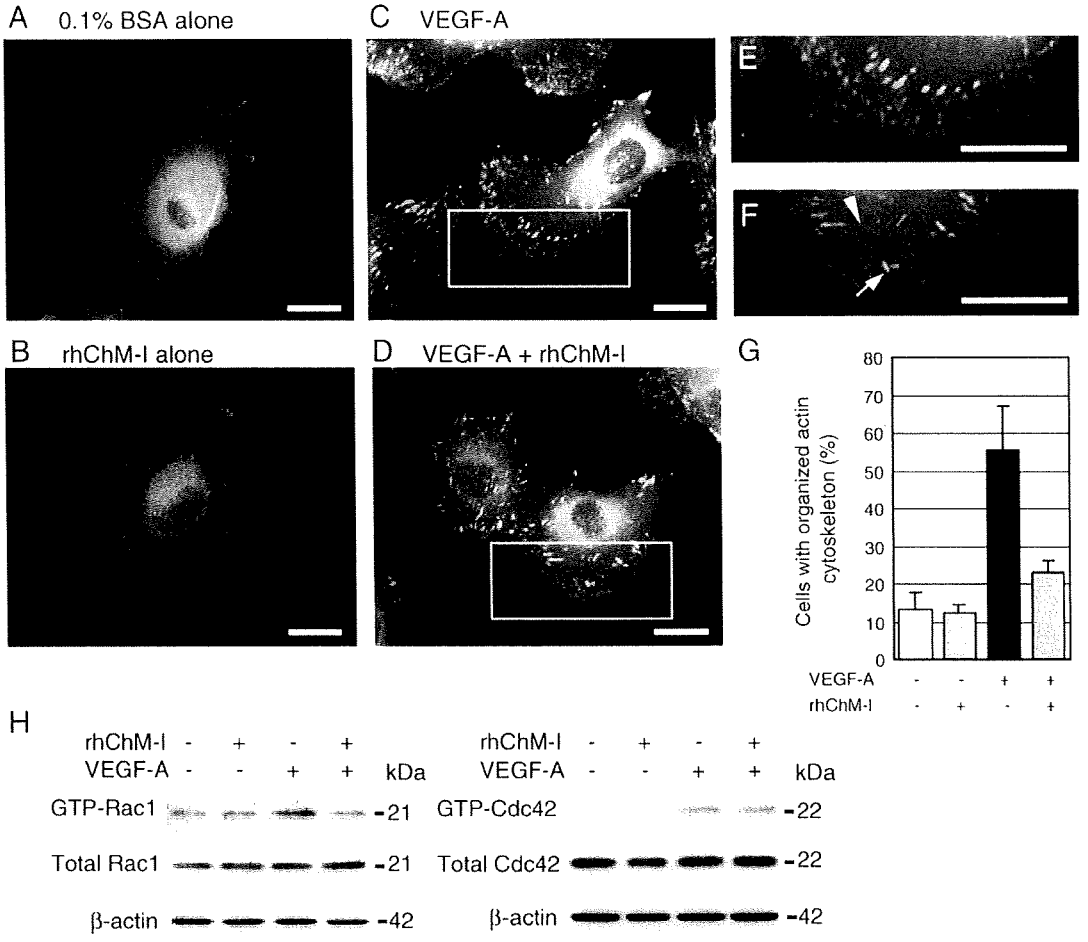

Fig. 6 – Effects of rhChM-I on the VEGF-A-induced reorganization of actin cytoskeleton in HUVECs. (A–F) Cells were cultured overnight on vitronectin-coated glass chamber slides, serum-starved for 5 h, and preincubated with 0.1% BSA/PBS (A and C) or rhChM-I (1 μg/ml) (B and D) for 30 min. The cells were then stimulated with VEGF-A (25 ng/ml) (C–F) for 1 h, fixed, permeabilized, and immunostained. Focal adhesions (*green*) were visualized with anti-paxillin antibody followed by incubation with an Alexa Fluor 488-conjugated secondary antibody. Actin filaments (*red*) and nuclei (*blue*) were stained with Alexa Fluor 594-conjugated phalloidin and DAPI, respectively. The photographs shown are merged images. The boxed areas in panels C and D are magnified in panels E and F, respectively. The arrowhead and arrow in panel F indicate the shorter actin filaments and the focal adhesion poorly linked to actin filaments, respectively. Bars, 20 μm. (G) Quantification of cells with an organized actin cytoskeleton. Values are the means ± SD of at least 200 randomly selected cells obtained in different fields from two independent experiments. (H) Effects of rhChM-I on VEGF-A-induced activation of Rac1 and Cdc42. HUVECs were serum-starved for 4 h and preincubated with or without rhChM-I (1 μg/ml) for 30 min. The cells were stimulated with VEGF-A (20 ng/ml) for 30 min (Rac1) or 10 min (Cdc42), lysed, and assayed for the activity of Rac1 and Cdc42 as described in Fig. 5. Equal loading of the samples was verified by an anti-β-actin antibody. The results shown are the representative of three independent experiments.

paxillin antibody, respectively. In unstimulated HUVECs, phalloidin and paxillin immunostaining were diffuse with weak cytoplasmic staining and rhChM-I had little effects on such a static actin cytoskeleton (Figs. 6A and B). Treatment of cells with VEGF-A induced a marked actin cytoskeletal reorganization characterized by an increased number of transcytoplasmic actin filaments anchored to large focal adhesions (Fig. 6C). These cells exhibited a broad lamellipodium with organized actin cytoskeleton (Figs. 6C and E). Cotreatment of the cells with rhChM-I and VEGF-A resulted in an apparent decrease in transcytoplasmic actin filaments but had relatively little effect on the assembly of large focal adhesions. Instead, focal adhesions together with the remaining shorter actin filaments were irregularly oriented and poorly linked to each other in the lamellipodium of the rhChM-I-treated cells (Fig. 6F, arrow and arrowhead), leading to the increased number of cells with a disrupted actin cytoskeleton (Fig. 6G).

It has been shown that the activity of Rac1 and Cdc42 are stimulated by VEGF-A and are involved in the VEGF-A-induced actin cytoskeletal reorganization and migration of endothelial cells [34,35]. We next examined whether rhChM-I inhibits the VEGF-A-induced activation of Rac1 and Cdc42. As previously

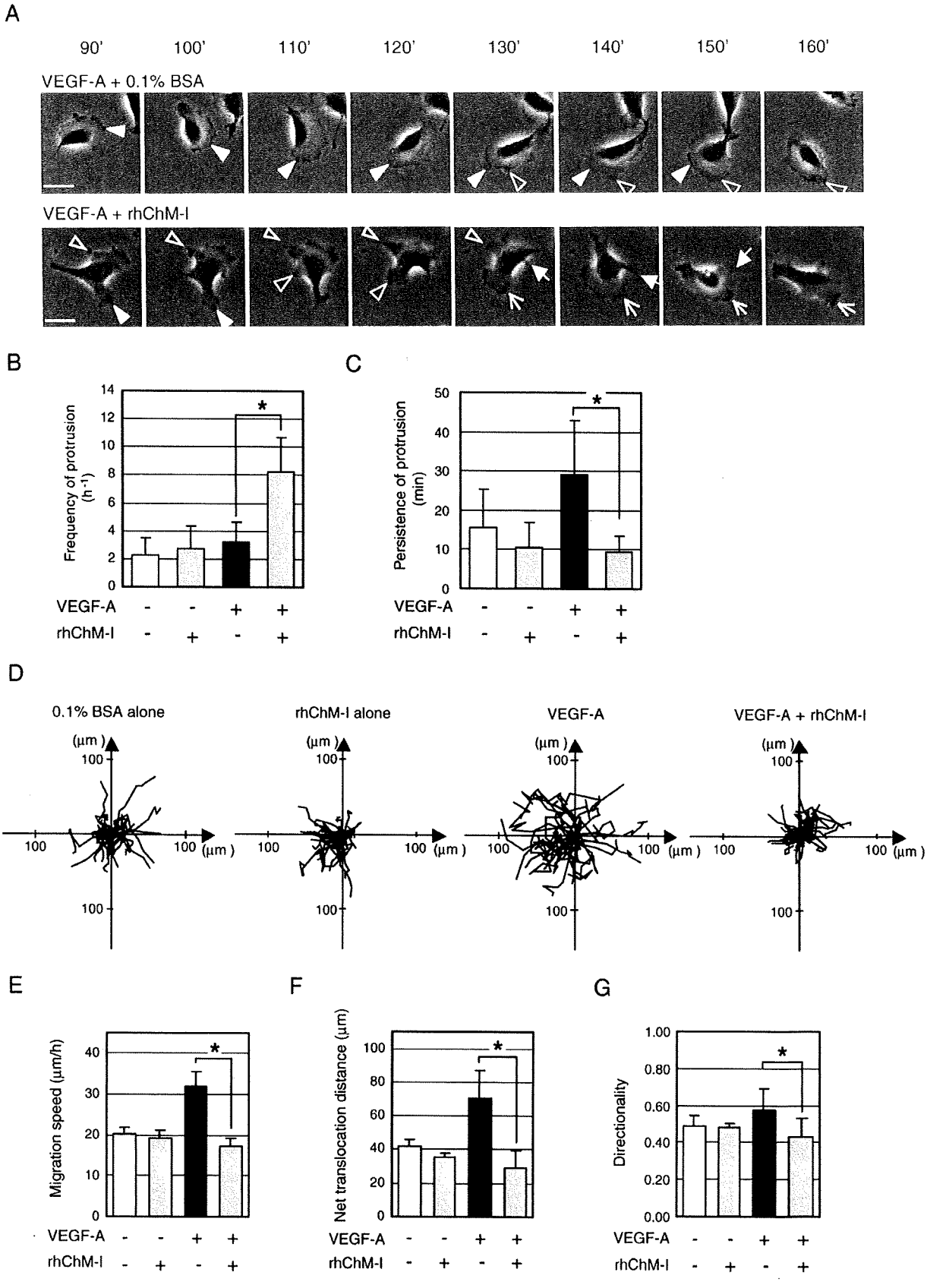
A
90'
100'
110'
120'
130'
140'
150'
160'
VEGF-A + 0.1% BSA
VEGF-A + rhChM-I
B
Frequency of protrusion (h-1)
VEGF-A
rhChM-I
C
Persistence of protrusion (min)
VEGF-A
rhChM-I
D
0.1% BSA alone
rhChM-I alone
VEGF-A
VEGF-A + rhChM-I
(μm)
E
Migration speed (μm/h)
VEGF-A
rhChM-I
F
Net translocation distance (μm)
VEGF-A
rhChM-I
G
Directionality
VEGF-A
rhChM-I

reported [34,35], treatment of serum-starved HUVECs with VEGF-A induced the activation of Rac1 and Cdc42 within 30 or 10 min, respectively. Recombinant human ChM-I completely blocked the VEGF-A-induced activation of Rac1, but not Cdc42. There were little effects on the basal activity of Rac1 and Cdc42 (Fig. 6H). Consistent with the reduced activity of Rac1, VEGF-A-induced Ser-3 phosphorylation of cofilin, an actin depolymerizing factor downstream of Rac1, was also inhibited by rhChM-I in HUVECs and MSS31 cells, which leads to the enhanced actin depolymerization by cofilin (Figs. S5A–D).

Effects of rhChM-I on the VEGF-A-stimulated lamellipodial extensions and cell motility in HUVECs

Using time-lapse video microscopy, we performed tracking analysis of VEGF-A-stimulated cells in sparse culture. Serum-starved HUVECs were stimulated by the addition of VEGF-A (25 ng/ml) in the presence or absence of rhChM-I (Fig. 7A). Cells stimulated by VEGF-A exhibited smooth and stable lamellipodia that extended toward the moving direction. In contrast, HUVECs treated with rhChM-I exhibited less polarized morphologies due to the formation of multiple cell protrusions at a single time. Quantification of the frequency and persistence of the protrusions revealed that although VEGF-A had little effect on the frequency of protrusions, it increased the persistence of protrusions by 1.9-fold. Treatment of HUVECs with rhChM-I apparently increased the frequency of protrusions, and decreased their persistence in the presence of VEGF-A but had no significant effects on those of the unstimulated cells (Figs. 7B and C, $n=75$). This indicates that rhChM-I prevents the persistent extension of cell protrusions that give rise to a stable lamellipodium functioning as a leading edge. By tracking the migration of individual cells over a 4-h period of observation, migration tracks were generated (Fig. 7D). Migration speeds, the net translocation distance, and the directionality were then calculated (Figs. 7E–G, $n=75$). VEGF-A increased the average migration speed and the net translocation distance by 1.6-fold and 1.7-fold, respectively. Treatment of HUVECs with rhChM-I in the presence of VEGF-A suppressed this VEGF-A-stimulated motility of HUVECs to the basal levels (Figs. 7E and F). Moreover, rhChM-I reduced the directionality of cell migration stimulated by VEGF-A (Fig. 7G). The directional migration of HUVECs in an *in vitro* wound-healing migration model was also inhibited by rhChM-I and the assembly of actin filaments and focal adhesions were disturbed at the leading edge of the cells (Figs. S5E–H). Thus, in the presence of rhChM-I, cells move slowly and frequently turn their moving direction. These data suggest that ChM-I impairs the motility of VEGF-A-stimulated HUVECs by preventing the formation of stable lamellipodial extensions.

Discussion

We expressed rhChM-I as a secretable form in 293-F cells and confirmed its anti-angiogenic activity by verifying its inhibition of mouse corneal angiogenesis (Table 1 and Fig. 1). Using this preparation of rhChM-I, we analyzed its effects on VEGF-A-induced endothelial cell migration, an essential step in angiogenesis, in our present study. Our results indicate that rhChM-I inhibits the VEGF-A-induced chemotactic migration of HUVECs by 70–80% but has no effect upon the basal migration of non-stimulated HUVECs (Fig. 2). It also effectively inhibited the VEGF-A-induced chemotactic migration of HUVECs (ID_{50}, ~5.4 nM) in a modified Boyden chamber assay (Fig. 2), as commonly seen for angiogenesis inhibitors such as thrombospondin-1 (TSP-1), angiostatin, and endostatin [26,36,37].

A blockade of the signal entry from integrins and growth factor receptors is a possible mechanism accounting for the inhibitory actions of ChM-I upon angiogenesis. For many angiogenesis inhibitors such as endostatin, arresten, and endorepellin, their binding to integrins interferes with the adhesion of vascular endothelial cells and triggers the signaling events including FAK phosphorylation, which leads to the inhibition of cell migration [38-41]. However, as demonstrated in Figs. 5A and B and Fig. S3C, pretreatment of HUVECs with rhChM-I affected neither adhesion of HUVECs to any of the ECM proteins tested nor the phosphorylation of FAK in the adhering or quiescent HUVECs. Moreover, even in the presence of the maximal dose of the function-blocking antibodies against integrin β1 or αvβ3 (Fig. S4), rhChM-I further inhibited the VEGF-A-induced migration of HUVECs, suggesting that the inhibitory actions of ChM-I occur independently of integrin-mediated cell adhesion. The disruption of integrin-mediated adhesion thus appears not to be the target of ChM-I actions.

With regards to the signal entry from VEGF-A, we detected no alterations in the VEGF-A-induced phosphorylation of VEGFR-2 and its downstream signaling molecule ERK1/2, c-Src, and FAK in rhChM-I-treated HUVECs (Figs. S3A-C), indicating that the ChM-I action is not simply mediated by the inhibition of VEGFR-2 signal entry. In fact, rhChM-I similarly inhibited the chemotactic migration of HUVECs induced via the FGF-2 and IGF-I RTK pathways. Interestingly, ChM-I had no inhibitory effects on migration stimulated by PMA through a PKC pathway or by S1P through a GPCR pathway (Fig. 3). Moreover, although FGF-2 is a potent stimulator of migration in a wide variety of FGFR

Fig. 7 – Effects of rhChM-I on the motility of HUVECs stimulated by VEGF-A. Serum-starved HUVECs were plated on vitronectin-coated dishes and allowed to adhere for 1 h. The cells were preincubated with or without rhChM-I (0.5 μg/ml) in αMEM containing 0.5% FBS for 30 min and then stimulated with VEGF-A (25 ng/ml), as described. Cell migration was monitored for 4 h at 2 min intervals. (A) Typical time-lapse phase-contrast micrographs of control and rhChM-I-treated cells at 90–160 min after the addition of VEGF-A. Arrows and arrowheads indicate extending lamellipodia or cell protrusions. Bars, 30 μm. (B, C) The frequency (B) and persistence (C) of the protrusions were quantified at 120–180 min after the addition of VEGF-A. Values are the means ± SD ($n=75$) from four independent experiments. *$P<0.05$. (D) Migration tracks of HUVECs in the presence and absence of rhChM-I. The tracks during a total observation period of 4 h were generated by marking the position of the nucleus at every 30 min interval for each cell. Migration tracks obtained from 30 cells in each experimental condition were shown. (E–G) The migration speed (E), the net translocation distance (F), and the directionality (G) of the cells were measured on the basis of the migration tracks. Values are the means ± SD ($n=75$) from four independent experiments. *$P<0.05$.

responsive cells, including fibroblastic cell types, rhChM-I could only inhibit the FGF-2-induced migration of vascular endothelial cells (Fig. 4). The inhibitory action of rhChM-I is also evident in the FGF-2-induced migration of endothelial MSS31 cells. The mode of ChM-I actions on the signal pathways through RTKs and its narrow cell type selectivity are indicative of its unique action mechanism.

The activation of cell motility is an important component in chemotactic cell migration during the angiogenic responses of endothelial cells caused by VEGF-A [32]. Tracking analysis of HUVECs using time-lapse video microscopy revealed that, even in the absence of a concentration gradient, the migration speed and net translocation distance and the directionality of VEGF-A-stimulated HUVEC migration were significantly reduced to the basal level by rhChM-I, and that the cells altered their moving direction more frequently in the presence of rhChM-I (Figs. 7D–G). These results indicate that ChM-I suppresses the VEGF-A-stimulated motility of endothelial cells, particularly their directional mode of motility. A broad single lamellipodium is characteristic of cells undergoing active and stable directional migration, as seen in VEGF-A-stimulated HUVECs (Fig. 7A) [32]. In contrast, in the presence of rhChM-I, HUVECs displayed multiple cell protrusions that were found to be extremely transient and poorly spread (Figs. 7A and C), indicating that ChM-I prevented the persistent extension of lamellipodium that will provide a stable leading edge and forward cell movement. This is compatible with our finding that the inhibitory action of rhChM-I was PI3K-dependent during the chemotaxis processes induced by VEGF-A (Fig. S3D), as PI3K plays a key role in directional cell migration by regulating the polarized extension of lamellipodia via various actin regulators including Rac and cofilin [42,43].

Membrane protrusive activities are generated by the coordinated reorganization of the actin cytoskeleton in response to cell–matrix interactions and/or growth factor signaling [32]. Rac and Cdc42 are pivotal regulators of actin polymerization and participate in various cellular events including spreading, morphogenesis, and the formation of lamellipodia and filopodia. In particular, Cdc42 is a master regulator of cell polarity and is required for the restriction of Rac activity to the cell front or leading edge. Thus, the marked reduction of these GTPase activities during spreading of rhChM-I-treated HUVECs (Figs. 5E and F) suggests that actin reorganization, which promotes lamellipodial extension, is severely disturbed by the presence of ChM-I. This is consistent with the delayed cell spreading and the reduced number of cells with broad lamellipodia in rhChM-I-treated HUVECs (Figs. 5C and D). Furthermore, the confined localization of Rac1 to the front of the protrusions was observed to be poor in the rhChM-I-treated cells (data not shown). Hence, the formation of multiple but less spread protrusions caused by rhChM-I might be due to the partial loss of actin polymerizing activity with the concomitant loss of its polarity. In this regard, these protrusions are quite different from those formed in angiomotin-deficient endothelial cells, in which increased Rac activity induces multiple lamellipodia with polarization defects [44]. In addition, these actions of rhChM-I are likely to be effective when the cells dynamically reorganizes their actin cytoskeleton during cell spreading because the area of cell spreading and the number of cells with lamellipodia were gradually recovered up to 2 h after seeding (Figs. 5C and D).

VEGF-A stimulates the reorganization of actin filaments and focal adhesions in vascular endothelial cells. It has been reported that Rac1 is activated by VEGF-A and plays essential roles in VEGF-A-induced actin reorganization and cell migration. Our present data demonstrated that rhChM-I inhibited the VEGF-A-induced activity of Rac1, but not its basal activity (Fig. 6H). Consistent with this, Soga and coworkers [34] reported that Rac1 is indispensable, but Cdc42 is dispensable for the VEGF-A-induced endothelial cell chemotaxis. The reduced activity of Rac1 might be associated with the disrupted actin cytoskeleton and the disassembly of small focal adhesion called "focal complexes" as observed in the rhChM-I-treated HUVECs (Figs. 6D and F). Recently, Rac1 has been shown to affect the rate of actin depolymerization by inhibiting cofilin-induced actin depolymerization through a PAK-mediated pathway [45,46]. We also found that rhChM-I inhibits VEGF-A-induced Ser-3 phosphorylation of cofilin and possibly enhances the actin depolymerization in the HUVECs and the MSS31 cells (Figs. S5A–D). The partial decrease in the actin polymerization activity together with the enhanced depolymerization activity may probably affect the VEGF-A-stimulated dynamic extension of lamellipodia and the directional migration of cells. In fact, our time-lapse data revealed that rhChM-I impairs the stable extension of lamellipodia in VEGF-A-stimulated HUVECs (Figs. 7A–C). These effects of rhChM-I on the lamellipodial extension may underlie the reduced motility and directionality of cells stimulated by VEGF-A (Figs. 7D–G). Other angiogenesis inhibitors, such as endostatin, thrombospondin-1, fumagillin, and TNP-470, have been reported to decrease the number of lamellipodia with the increased number of actin stress fibers and the phosphorylation of cofilin in HUVECs as well as in human dermal microvascular endothelial cells [47]. These inhibitors induce a more adhesive state in cells with a static actin cytoskeleton, which is unfavorable for active motility. Hence, the mode of ChM-I action is fundamentally distinct from those of other known angiogenesis inhibitors.

Acknowledgments

We thank Dr. J. Miyazaki (Osaka University Medical School) for providing the pCAGGS expression vector. This work was supported by the Grants-in-aid from the Ministry of Education, Culture, Sports, Science, and Technology of Japan (Y.H.).

Appendix A. Supplementary data

Supplementary data associated with this article can be found, in the online version, at doi:10.1016/j.yexcr.2009.12.009.

REFERENCES

[1] J. Folkman, Angiogenesis in cancer, vascular, rheumatoid and other disease, Nat. Med. 1 (1995) 27–31.
[2] R. Kalluri, Basement membranes: structure, assembly and role in tumour angiogenesis, Nat. Rev., Cancer 3 (2003) 422–433.
[3] M.S. O'Reilly, T. Boehm, Y. Shing, N. Fukai, G. Vasios, W.S. Lane, E. Flynn, J.R. Birkhead, B.R. Olsen, J. Folkman, Endostatin: an endogenous inhibitor of angiogenesis and tumor growth, Cell 88 (1997) 277–285.

[4] T.M. Mundel, R. Kalluri, Type IV collagen-derived angiogenesis inhibitors, Microvasc. Res 74 (2007) 85–89.
[5] Y. Hiraki, H. Tanaka, H. Inoue, J. Kondo, A. Kamizono, F. Suzuki, Molecular cloning of a new class of cartilage-specific matrix, chondromodulin-I, which stimulates growth of cultured chondrocytes, Biochem. Biophys. Res. Commun. 175 (1991) 971–977.
[6] C. Shukunami, Y. Hiraki, Chondromodulin-I and tenomodulin: the negative control of angiogenesis in connective tissue, Curr. Pharm. Des. 13 (2007) 2101–2112.
[7] Y. Hiraki, T. Kono, M. Sato, C. Shukunami, J. Kondo, Inhibition of DNA synthesis and tube morphogenesis of cultured vascular endothelial cells by chondromodulin-I, FEBS Lett. 415 (1997) 321–324.
[8] Y. Hiraki, H. Inoue, K. Iyama, A. Kamizono, M. Ochiai, C. Shukunami, S. Iijima, F. Suzuki, J. Kondo, Identification of chondromodulin I as a novel endothelial cell growth inhibitor. Purification and its localization in the avascular zone of epiphyseal cartilage, J. Biol. Chem. 272 (1997) 32419–32426.
[9] Y. Hiraki, K. Mitsui, N. Endo, K. Takahashi, T. Hayami, H. Inoue, C. Shukunami, K. Tokunaga, T. Kono, M. Yamada, H.E. Takahashi, J. Kondo, Molecular cloning of human chondromodulin-I, a cartilage-derived growth modulating factor, and its expression in Chinese hamster ovary cells, Eur. J. Biochem. 260 (1999) 869–878.
[10] C. Shukunami, K. Iyama, H. Inoue, Y. Hiraki, Spatiotemporal pattern of the mouse chondromodulin-I gene expression and its regulatory role in vascular invasion into cartilage during endochondral bone formation, Int. J. Dev. Biol. 43 (1999) 39–49.
[11] U.H. Dietz, G. Ziegelmeier, K. Bittner, P. Bruckner, R. Balling, Spatio-temporal distribution of chondromodulin-I mRNA in the chicken embryo: expression during cartilage development and formation of the heart and eye, Dev. Dyn. 216 (1999) 233–243.
[12] H. Funaki, S. Sawaguchi, K. Yaoeda, Y. Koyama, E. Yaoita, S. Funaki, M. Shirakashi, Y. Oshima, C. Shukunami, Y. Hiraki, H. Abe, T. Yamamoto, Expression and localization of angiogenic inhibitory factor, chondromodulin-I, in adult rat eye, Invest. Ophthalmol. Vis. Sci. 42 (2001) 1193–1200.
[13] M. Yoshioka, S. Yuasa, K. Matsumura, K. Kimura, T. Shiomi, N. Kimura, C. Shukunami, Y. Okada, M. Mukai, H. Shin, R. Yozu, M. Sata, S. Ogawa, Y. Hiraki, K. Fukuda, Chondromodulin-I maintains cardiac valvular function by preventing angiogenesis, Nat. Med. 12 (2006) 1151–1159.
[14] C. Shukunami, A. Takimoto, S. Miura, Y. Nishizaki, Y. Hiraki, Chondromodulin-I and tenomodulin are differentially expressed in the avascular mesenchyme during mouse and chick development, Cell Tissue Res. 332 (2008) 111–122.
[15] Y. Nakamichi, C. Shukunami, T. Yamada, K. Aihara, H. Kawano, T. Sato, Y. Nishizaki, Y. Yamamoto, M. Shindo, K. Yoshimura, T. Nakamura, N. Takahashi, H. Kawaguchi, Y. Hiraki, S. Kato, Chondromodulinl , is a bone remodeling factor, Mol. Cell. Biol. 23 (2003) 636–644.
[16] W. Risau, Mechanisms of angiogenesis, Nature 386 (1997) 671–674.
[17] H. Niwa, K. Yamamura, J. Miyazaki, Efficient selection for high-expression transfectants with a novel eukaryotic vector, Gene 108 (1991) 193–199.
[18] Y. Oshima, K. Sato, F. Tashiro, J. Miyazaki, K. Nishida, Y. Hiraki, Y. Tano, C. Shukunami, Anti-angiogenic action of the C-terminal domain of tenomodulin that shares homology with chondromodulin-I, J. Cell Sci. 117 (2004) 2731–2744.
[19] K. Watanabe, Y. Hasegawa, H. Yamashita, K. Shimizu, Y. Ding, M. Abe, H. Ohta, K. Imagawa, K. Hojo, H. Maki, H. Sonoda, Y. Sato, Vasohibin as an endothelium-derived negative feedback regulator of angiogenesis, J. Clin. Invest. 114 (2004) 898–907.
[20] N. Yanai, T. Satoh, M. Obinata, Endothelial cells create a hematopoietic inductive microenvironment preferential to erythropoiesis in the mouse spleen, Cell Struct. Funct. 16 (1991) 87–93.
[21] K. Namba, M. Abe, S. Saito, M. Satake, T. Ohmoto, T. Watanabe, Y. Sato, Indispensable role of the transcription factor PEBP2/CBF in angiogenic activity of a murine endothelial cell MSS31, Oncogene 19 (2000) 106–114.
[22] C. Shukunami, C. Shigeno, T. Atsumi, K. Ishizeki, F. Suzuki, Y. Hiraki, Chondrogenic differentiation of clonal mouse embryonic cell line ATDC5 in vitro: differentiation-dependent gene expression of parathyroid hormone (PTH)/PTH-related peptide receptor, J. Cell Biol. 133 (1996) 457–468.
[23] P. Chomczynski, N. Sacchi, Single-step method of RNA isolation by acid guanidinium thiocyanate-phenol-chloroform extraction, Anal. Biochem. 162 (1987) 156–159.
[24] S.A. Wickstrom, K. Alitalo, J. Keski-Oja, An endostatin-derived peptide interacts with integrins and regulates actin cytoskeleton and migration of endothelial cells, J. Biol. Chem. 279 (2004) 20178–20185.
[25] P. Nyberg, L. Xie, R. Kalluri, Endogenous inhibitors of angiogenesis, Cancer Res 65 (2005) 3967–3979.
[26] N. Yamaguchi, B. Anand-Apte, M. Lee, T. Sasaki, N. Fukai, R. Shapiro, I. Que, C. Lowik, R. Timpl, B.R. Olsen, Endostatin inhibits VEGF-induced endothelial cell migration and tumor growth independently of zinc binding, EMBO J. 18 (1999) 4414–4423.
[27] R. Montesano, L. Orci, Tumor-promoting phorbol esters induce angiogenesis in vitro, Cell 42 (1985) 469–477.
[28] D. English, Z. Welch, A.T. Kovala, K. Harvey, O.V. Volpert, D.N. Brindley, J.G. Garcia, Sphingosine 1-phosphate released from platelets during clotting accounts for the potent endothelial cell chemotactic activity of blood serum and provides a novel link between hemostasis and angiogenesis, FASEB J. 14 (2000) 2255–2265.
[29] F. Wang, J.R. Van Brocklyn, J.P. Hobson, S. Movafagh, Z. Zukowska-Grojec, S. Milstien, S. Spiegel, Sphingosine 1-phosphate stimulates cell migration through a G(i)-coupled cell surface receptor. Potential involvement in angiogenesis, J. Biol. Chem. 274 (1999) 35343–35350.
[30] B. Boilly, A.S. Vercoutter-Edouart, H. Hondermarck, V. Nurcombe, X. Le Bourhis, FGF signals for cell proliferation and migration through different pathways, Cytokine Growth Factor Rev. 11 (2000) 295–302.
[31] M.B. Calalb, T.R. Polte, S.K. Hanks, Tyrosine phosphorylation of focal adhesion kinase at sites in the catalytic domain regulates kinase activity: a role for Src family kinases, Mol. Cell. Biol. 15 (1995) 954–963.
[32] A.J. Ridley, M.A. Schwartz, K. Burridge, R.A. Firtel, M.H. Ginsberg, G. Borisy, J.T. Parsons, A.R. Horwitz, Cell migration: integrating signals from front to back, Science 302 (2003) 1704–1709.
[33] H. Abedi, I. Zachary, Vascular endothelial growth factor stimulates tyrosine phosphorylation and recruitment to new focal adhesions of focal adhesion kinase and paxillin in endothelial cells, J. Biol. Chem. 272 (1997) 15442–15451.
[34] N. Soga, N. Namba, S. McAllister, L. Cornelius, S.L. Teitelbaum, S.F. Dowdy, J. Kawamura, K.A. Hruska, Rho family GTPases regulate VEGF-stimulated endothelial cell motility, Exp. Cell Res. 269 (2001) 73–87.
[35] T.A. Garrett, J.D. Van Buul, K. Burridge, VEGF-induced Rac1 activation in endothelial cells is regulated by the guanine nucleotide exchange factor Vav2, Exp. Cell Res. 313 (2007) 3285–3297.
[36] W.R. Ji, F.J. Castellino, Y. Chang, M.E. Deford, H. Gray, X. Villarreal, M.E. Kondri, D.N. Marti, M. Llinas, J. Schaller, R.A. Kramer, P.A. Trail, Characterization of kringle domains of angiostatin as antagonists of endothelial cell migration, an important process in angiogenesis, FASEB J 12 (1998) 1731–1738.
[37] S.M. Short, A. Derrien, R.P. Narsimhan, J. Lawler, D.E. Ingber, B.R. Zetter, Inhibition of endothelial cell migration by thrombospondin-1 type-1 repeats is mediated by beta1 integrins, J. Cell Biol. 168 (2005) 643–653.
[38] J. Dixelius, M. Cross, T. Matsumoto, T. Sasaki, R. Timpl, L. Claesson-Welsh, Endostatin regulates endothelial cell adhesion

and cytoskeletal organization, Cancer Res. 62 (2002) 1944–1947.
[39] A. Sudhakar, H. Sugimoto, C. Yang, J. Lively, M. Zeisberg, R. Kalluri, Human tumstatin and human endostatin exhibit distinct antiangiogenic activities mediated by alpha v beta 3 and alpha 5 beta 1 integrins, Proc. Natl. Acad. Sci. U. S. A. 100 (2003) 4766–4771.
[40] G. Bix, J. Fu, E.M. Gonzalez, L. Macro, A. Barker, S. Campbell, M.M. Zutter, S.A. Santoro, J.K. Kim, M. Hook, C.C. Reed, R.V. Iozzo, Endorepellin causes endothelial cell disassembly of actin cytoskeleton and focal adhesions through alpha2beta1 integrin, J. Cell Biol. 166 (2004) 97–109.
[41] A. Sudhakar, P. Nyberg, V.G. Keshamouni, A.P. Mannam, J. Li, H. Sugimoto, D. Cosgrove, R. Kalluri, Human alpha1 type IV collagen NC1 domain exhibits distinct antiangiogenic activity mediated by alpha1beta1 integrin, J. Clin. Invest. 115 (2005) 2801–2810.
[42] V. Kolsch, P.G. Charest, R.A. Firtel, The regulation of cell motility and chemotaxis by phospholipid signaling, J. Cell Sci. 121 (2008) 551–559.
[43] M. Vicente-Manzanares, C.K. Choi, A.R. Horwitz, Integrins in cell migration—the actin connection, J. Cell Sci. 122 (2009) 199–206.
[44] K. Aase, M. Ernkvist, L. Ebarasi, L. Jakobsson, A. Majumdar, C. Yi, O. Birot, Y. Ming, A. Kvanta, D. Edholm, P. Aspenstrom, J. Kissil, L. Claesson-Welsh, A. Shimono, L. Holmgren, Angiomotin regulates endothelial cell migration during embryonic angiogenesis, Genes Dev. 21 (2007) 2055–2068.
[45] A.J. Ridley, Rho GTPases and cell migration, J. Cell Sci. 114 (2001) 2713–2722.
[46] M. Vicente-Manzanares, D.J. Webb, A.R. Horwitz, Cell migration at a glance, J. Cell Sci. 118 (2005) 4917–4919.
[47] S.M. Keezer, S.E. Ivie, H.C. Krutzsch, A. Tandle, S.K. Libutti, D.D. Roberts, Angiogenesis inhibitors target the endothelial cell cytoskeleton through altered regulation of heat shock protein 27 and cofilin, Cancer Res 63 (2003) 6405–6412.

Laboratory Investigation (2010) 90, 52–60

Acyclic retinoid inhibits angiogenesis by suppressing the MAPK pathway

Yusuke Komi[1,2], Yukihisa Sogabe[1], Naoto Ishibashi[3], Yasufumi Sato[4], Hisataka Moriwaki[5], Kentaro Shimokado[2] and Soichi Kojima[1]

Acyclic retinoid (ACR) is currently under clinical trial as an agent to suppress the recurrence of hepatocellular carcinoma (HCC) through its ability to induce apoptosis in premature HCC cells. ACR has an anticancer effect *in vivo* as well, although it shows weak apoptosis-inducing activity against mature HCC cells, suggesting the existence of an additional action mechanism. In this study, we investigated the antiangiogenic activity of ACR. ACR inhibited angiogenesis within chicken chorioallantoic membrane (CAM) in as similar a manner as all-*trans* retinoic acid (atRA). Although suppression of angiogenesis by atRA was partially rescued by the simultaneous addition of angiopoietin-1, suppression of angiogenesis by ACR was not rescued under the same condition at all. Conversely, although suppression of angiogenesis by ACR was partially inverted by the simultaneous addition of vascular endothelial growth factor (VEGF), suppression of angiogenesis by atRA was not affected under the same condition. These results suggested that mechanisms underlying the suppression of angiogenesis by ACR and atRA were different. ACR selectively inhibited the phosphorylation of VEGF receptor 2 (VEGFR2) and of extracellular signal-regulated kinase (ERK) without changing their protein expression levels, and inhibited endothelial cell growth, migration, and tube formation. The inhibition of the phosphorylation of ERK, endothelial growth, migration, tube formation, and angiogenesis by ACR was rescued by the overexpression of constitutively active mitogen-activated protein kinase (MAPK). Finally, ACR, but not atRA, inhibited HCC-induced angiogenesis in a xenografted CAM model. These results delineate the novel activity of ACR as an antiangiogenic through a strong inhibition of the VEGFR2 MAPK pathway.

Laboratory Investigation (2010) **90,** 52–60; doi:10.1038/labinvest.2009.110; published online 19 October 2009

KEYWORDS: ACR; HCC; MAPK pathway; phosphorylation; tumor angiogenesis; VEGF receptor

Angiogenesis has an important role in tumor growth by supplying nutrients and providing a route for metastasis.[1] Therefore, tumor angiogenesis is a good target for the treatment of solid cancers. Tumor cells induce angiogenesis by producing and releasing several angiogenic factors, such as vascular endothelial growth factor (VEGF), basic fibroblast growth factor (bFGF), and angiopoietins (Angs).[1] The VEGF/VEGF receptor (VEGFR) signaling pathway is essential for drawing endothelial cells from preexisting blood vessels and in stimulating their growth,[2] whereas the Ang/Tie2 signaling pathway is important for sustaining the interaction between endothelial and mural cells and stabilizing the vasculature.

Retinoids (vitamin A and its derivatives) are natural fat-soluble hormones, the biological effects of which are believed to be mediated, all or in part, by the modulation of target gene expression through two families of nuclear receptors: retinoic acid receptors (RARs) and retinoid X receptors (RXRs).[3] Retinoids exert antitumor activity by modifying the transactivation of $p21^{CIP1}$, interferon receptor, and signal transduction and activator of transcription.[4,5] We previously reported that all-*trans* retinoic acid (atRA) inhibits angiogenesis on chorioallantoic membrane (CAM) through disruption of vascular remodeling by inducing Ang2 expression and suppressing Ang/Tie2 signaling.[6] Acyclic retinoid (ACR)

[1]Molecular Ligand Biology Research Team, Chemical Genomics Research Group, Chemical Biology Department, RIKEN Advanced Science Institute, Saitama, Japan; [2]Department of Vascular Medicine and Geriatrics, Tokyo Medical and Dental University Graduate School, Tokyo, Japan; [3]Tokyo New Drug Research Laboratory, Pharmaceutical Division, Kowa, Tokyo, Japan; [4]Department of Vascular Biology, Institute of Development, Aging and Cancer, Tohoku University, Sendai, Japan and [5]Department of Gastroenterology, Gifu University School of Medicine, Gifu, Japan

Correspondence: Professor S Kojima, PhD, Molecular Ligand Biology Research Team, Chemical Genomics Research Group, Chemical Biology Department, RIKEN Advanced Science Institute, 2-1 Wako, Saitama 351-0198, Japan.
E-mail: skojima@postman.riken.go.jp

Received 3 February 2009; revised 20 July 2009; accepted 31 July 2009

is a synthetic retinoid and activates the RAR and RXR.[7] Oral administration of ACR for 12 months significantly reduced the incidence of post-therapeutic recurrence of hepatocellular carcinoma (HCC) compared with the placebo group.[8] In this study, ACR did not cause the typical toxic effects observed with conventional retinoids.[8] Now, ACR is under clinical trials as a chemopreventive drug against the recurrence of HCC. Nuclear receptor RXR in HCC is highly phosphorylated through the Ras-extracellular signal-regulated kinase (ERK) pathway, inactivated, and accumulates in the line as a dominant-negative receptor.[9,10] ACR inhibits the phosphorylation of RXR by inactivating the Ras-ERK pathway, recovering transactivation by retinoic acid, and induces apoptosis in human HCC cell lines.[9,10] ACR also has an anticancer effect *in vivo*.[11] However, it exerts only weak apoptosis-inducing activity against mature HCC cells *in vivo*. This result suggests an existence of an additional molecular mechanism underlying the anticancer effect of ACR. Therefore, we predicted that ACR might have antiangiogenic activity.

Herein, we found that in contrast to the antiangiogenic mechanism of atRA, ACR inhibited angiogenesis through the inhibition of the VEGF receptor mitogen-activated protein kinase (MAPK) pathway. Moreover, ACR suppressed HCC-induced angiogenesis in a xenografted CAM model. These results suggest that ACR will also be clinically useful as an antiangiogenic agent, in addition to its current usage as a chemopreventive agent.

MATERIALS AND METHODS

Reagents

Acyclic retinoid (2E,4E,6E,10E)-3,7,11,15-tetramethylhexadeca-2,4,6,10,14-pentaenoic acid) was provided by Kowa (Tokyo, Japan). AtRA was purchased from Sigma-Aldrich (St Louis, MO, USA). ACR was dissolved in ethanol and dimethyl sulfoxide (DMSO) to yield stock solutions of 10 mM and 1 M, respectively, whereas atRA was dissolved in ethanol to yield a stock solution of 17 mM.

Chicken CAM Assay

In vivo antiangiogenic activity of ACR and atRA was assessed by CAM assay as described previously.[12] In brief, fertilized Dekalb chicken eggs (Omiya Kakin, Saitama, Japan) were placed in a humidified egg incubator. After a 4.5-day incubation at 38°C, a 1% solution of methylcellulose containing ACR or atRA at various concentrations was loaded inside a silicon ring that was placed onto the surface of CAM. After a further incubation for 2 days, a fat emulsion was injected into the chorioallantois, so that the vascular networks stood out against the white background of the lipid. Antiangiogenic responses were evaluated under a stereomicroscope and photographed with a $\times 7.25$ objective. Quantitative analyses were carried out with angiogenesis-measuring software (ver.2.0; KURABO, Osaka, Japan).[12]

Matrigel Plug Assay

Matrigel (BD Biosciences, Bedford, MA, USA) was mixed with 200 units/ml heparin (Nacalai Tesque, Kyoto, Japan), with and without 50 ng/ml VEGF (Pepro Tech, Rocky Hill, NJ, USA) and 5 μM ACR in 0.1% DMSO. The matrigel mixture was injected subcutaneously into 5-week-old female C57BL/6 mice (Charles River, Yokohama, Japan). The mice were killed 7 days later. The matrigel plugs were removed and fixed in 4% paraformaldehyde for 4 h, dehydrated through a graded ethanol series, and embedded in paraffin (Nacalai Tesque). Vertical sections (5 μm) were mounted on slides and stained with hematoxylin and eosin, and observed under an inverted microscope (model DM IRB, Leica Microsystems, Wetzlar, Germany).

Cell Cultures

Human umbilical vein endothelial cells (HUVECs) and bovine aortic endothelial cells were cultured as described.[12] HepG2 cells, human HCC, were cultured in Dulbecco's modified Eagle's medium (Sigma-Aldrich) supplemented with 10% fetal calf serum.

Transfection and Luciferase Assay

Transfection into HUVECs was carried out using a combination of LipofectAMINE 2000 Plus reagent (Invitrogen) and a constitutively active MAPK kinase vector (1.5 μg each per 35-mm dish).[13]

Western Blotting Analysis

After rinsing several times with TBS (20 mM Tris–HCl, 137 mM NaCl), cells were lysed in 1% Triton X-100 in 20 mM HEPES, pH 6.8, containing Complete protease inhibitor cocktail (1 tablet per 50 ml; Roche, Indianapolis, IN, USA), 1 mM EDTA, 1 mM PMSF, and 0.5 mM Na_3VO_5, and directly subjected to western analysis using phospho-VEGFR2-specific antibodies (1:1000 dilution; Cell Signaling Technology, Danvers, MA, USA), phospho-FGFR1-specific antibodies (1:1000 dilution; Cell Signaling Technology), or phospho-ERK-specific antibodies (1:2000 dilution, Cell Signaling Technology). Cell lysates were also subjected to western analysis using antibodies to VEGFR2, FGFR1, and ERK. Immunoreactive bands of proteins were detected with ECL-Plus chemiluminescence reagents (GE Healthcare, Buckinghamshire, UK).

In Vitro Tube Formation Assay

Tube formation by HUVECs on matrigel was assessed as described previously.[14] Unpolymerized matrigel (Becton Dickinson, Bedford, MA, USA) was diluted to a final concentration of 5 mg/ml with MCDB-131 medium, aliquoted 150 μl each into 24-well plates, and allowed to polymerize for 30 min at 37°C. HUVECs were transfected with a constitutively active MAPK kinase-expressing vector. Two days later, HUVECs were seeded onto the polymerized gel at 2×10^5 cells/well; thereafter, 100 ng/ml VEGF, 1 μM, 5 μM,

and 10 μM ACR and/or atRA were added, and incubated for 6 h. *In vitro* tube formation was examined under a phase-contrast microscope and photographed with a × 10 objective.

HCC-Induced Angiogenesis in a Xenografted CAM Model

Hepatocellular carcinoma-induced angiogenesis in a xenografted CAM model was assessed as previously described.[15,16] HepG2 cell suspensions with or without 5 μM ACR or atRA were delivered at 4×10^5 cells per embryo onto the top of the CAM on day 8 using a gelatin sponge, called Gelform (Pfizer, New York, NY, USA) implant. After a further 4-day incubation, a fat emulsion was injected into the chorioallantois, so that the vascular networks stood out against the white background of the lipid. Antiangiogenic responses were evaluated under a stereomicroscope and photographed with a × 25.

Statistical Analysis

Data are expressed as means ± s.d. Statistical significance was assessed by one-way analysis of variance, followed by Shaffer's *t*-test.

RESULTS

Comparison Between the Effects of ACR and atRA on Blood Vessel Formation in CAM

To determine whether ACR could inhibit *in vivo* angiogenesis, we carried out CAM assay (Figure 1). The formation of intricate vascular networks, developing within control CAM

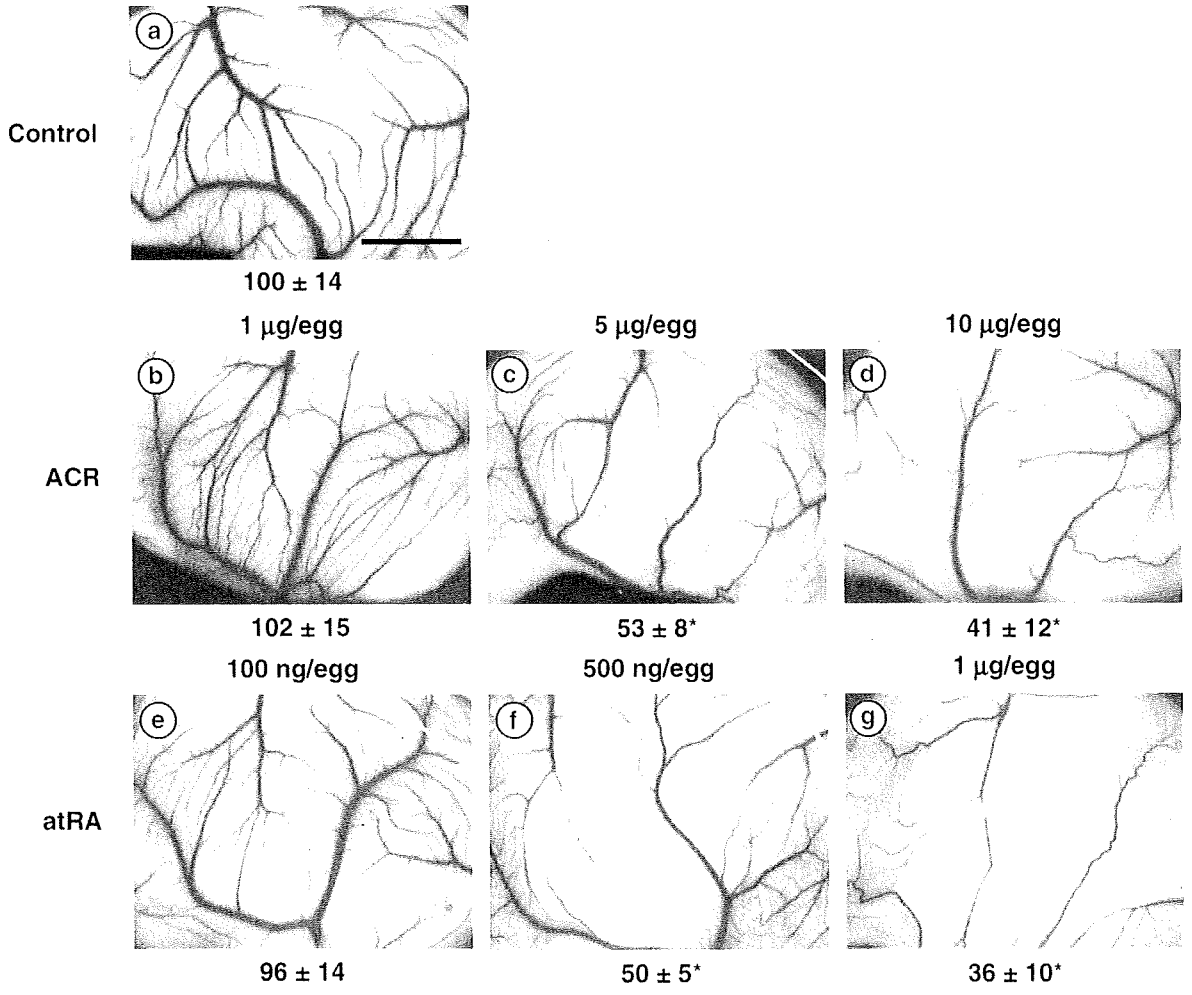

Figure 1 Suppression of *in vivo* angiogenesis in CAM by ACR and atRA. The 4.5-day-old CAMs were treated with ACR and atRA for 48 h, and then patterns of angiogenesis were photographed. Panel (**a**), vehicle (1% ethanol plus 1% DMSO); panel (**b**), 1 μg/egg ACR; panel (**c**), 5 μg/egg ACR; panel (**d**), 10 μg/egg ACR; panel (**e**), 100 ng/egg atRA; panel (**f**), 500 ng/egg atRA; panel (**g**), 1 μg/egg atRA. Scale bar, 5 mm. Total numbers of branches of blood vessels were analyzed with angiogenesis-measuring software and are shown under each panel. A total of 12 eggs (6 eggs per experiment × 2 experiments) were evaluated and representative results are shown. An asterisk indicates a significant difference ($P<0.05$) from the control.

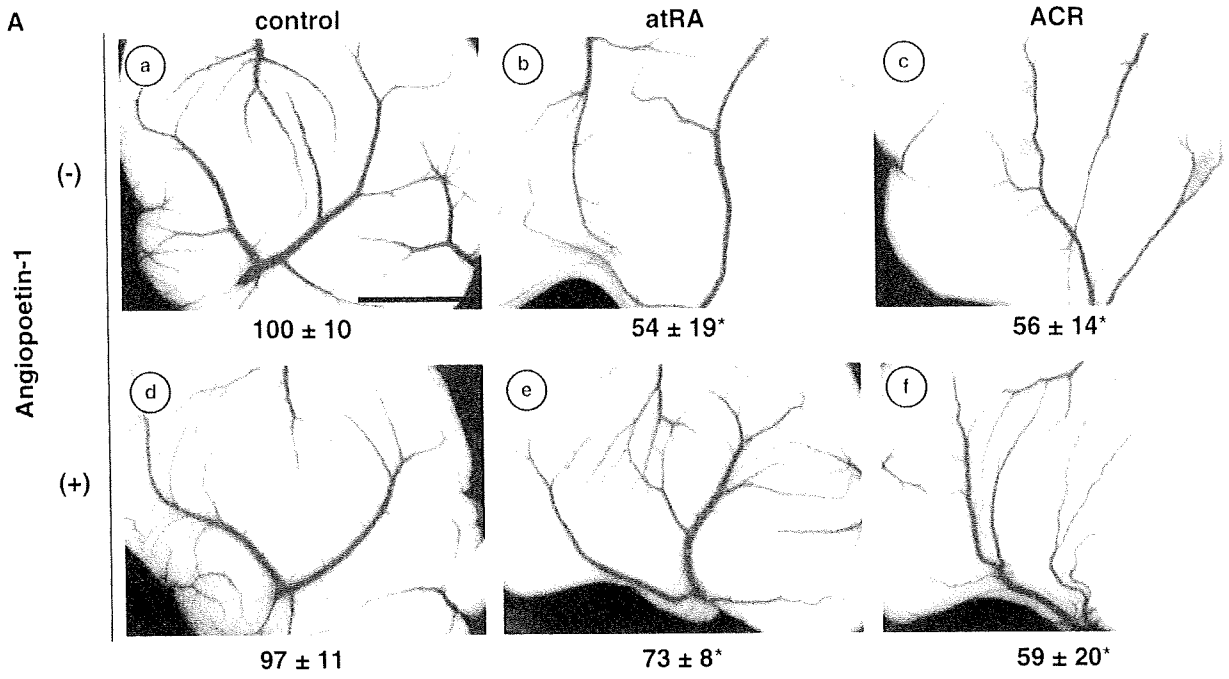

Figure 2 The antiangiogenic effect of atRA, but not ACR, was rescued by simultaneous treatment with Ang1 in CAM. (**A**) The 4.5-day-old CAMs were treated with ACR and atRA for 48 h and then patterns of angiogenesis were photographed. Panel (**a**), vehicle (1% ethanol plus 1% DMSO); panel (**b**), 500 ng/egg atRA; panel (**c**), 3 μg/egg ACR; panel (**d**), vehicle plus 300 ng/egg human recombinant Ang1; panel (**e**), 500 ng/egg atRA plus 300 ng/egg human recombinant Ang1; panel (**f**), 3 μg/egg ACR plus 300 ng/egg human recombinant Ang1. Scale bar, 5 mm. Total numbers of branches of blood vessels were analyzed with angiogenesis-measuring software and are shown under each panel. A total of 18 eggs (6 eggs per experiment × 3 experiments) were evaluated and representative results are shown. An asterisk indicates a significant difference ($P<0.05$) from the control. This result shows the representative result from three independent experiments, all of which gave similar results.

(Figure 1, panel a), was suppressed with ACR in a dose-dependent manner at concentrations of 1–10 μg/egg (0.3–3.3 mM inside the ring) (Figure 1, panels b–d) and with atRA in a dose-dependent manner at about 10 times lower concentrations of 100–1000 ng/egg (33–333 μM) (Figure 1, panels e–g). Although the inhibition of angiogenesis with atRA was partially rescued by simultaneous treatment with Angl at a concentration of 300 ng/egg as consistently as we reported previously[6] (Figure 2A, panel e), inhibition of angiogenesis with ACR was not rescued with Angl at all (Figure 2A, panel f). Furthermore, although atRA stimulated the transactivation activity of the *Ang2* promoter twofold (Supplementary Figure 1, column 2), ACR hardly showed such an activity (Supplementary Figure 1, columns 3 and 4). On the other hand, inhibition of angiogenesis with ACR, but not with atRA, was rescued by simultaneous treatment with VEGF (compare Figure 3A, panels e and f). To determine whether ACR might inhibit VEGF-induced blood vessel formation *in vivo*, we examined the effect of ACR in the matrigel plug assay (Figure 3B). Invasion of cells into gels was observed in the control matrigel that contained VEGF without ACR (panel a). When ACR was included in the matrigel at a concentration of 5 μM, the VEGF-induced invasion of cells was inhibited by about 54% (panel b).

Effect of ACR and atRA on Endothelial Cell Growth, Migration, and Tube Formation

We investigated the molecular mechanism by which ACR inhibited angiogenesis. First, we compared the effect of ACR and atRA on vascular endothelial cells. ACR (5 μM) suppressed the growth, migration, and tube formation (Figure 4A, lane 2, closed column; Figure 4B, lane 2, closed column; Figure 4C, panel b, respectively). These suppressive effects by ACR were, all or in part, rescued by overexpressing a constitutive active *MEK* gene (Figure 4A, lane 2, open column; Figure 4B, lane 2, open column; Figure 4C, panel e, respectively). Conversely, atRA did not suppress, rather it enhanced all of them (Figure 4A, lane 3, closed column; Figure 4B, lane 3, closed column; Figure 4C, panel c, respectively).

ACR Suppressed Phosphorylation of VEGFR2 and ERK

Next, we examined the effect of ACR and atRA on the phosphorylation of angiogenic growth factor receptors expressed by endothelial cells. As seen in the upper panel of Figure 5a, induction of phosphorylated 230 kD VEGFR2 after VEGF treatment was blocked to about 20% by pretreatment with 5 μM ACR for 24 h (compare lanes 4 with 5). In contrast, pretreatment with 5 μM atRA for 24 h did not block the

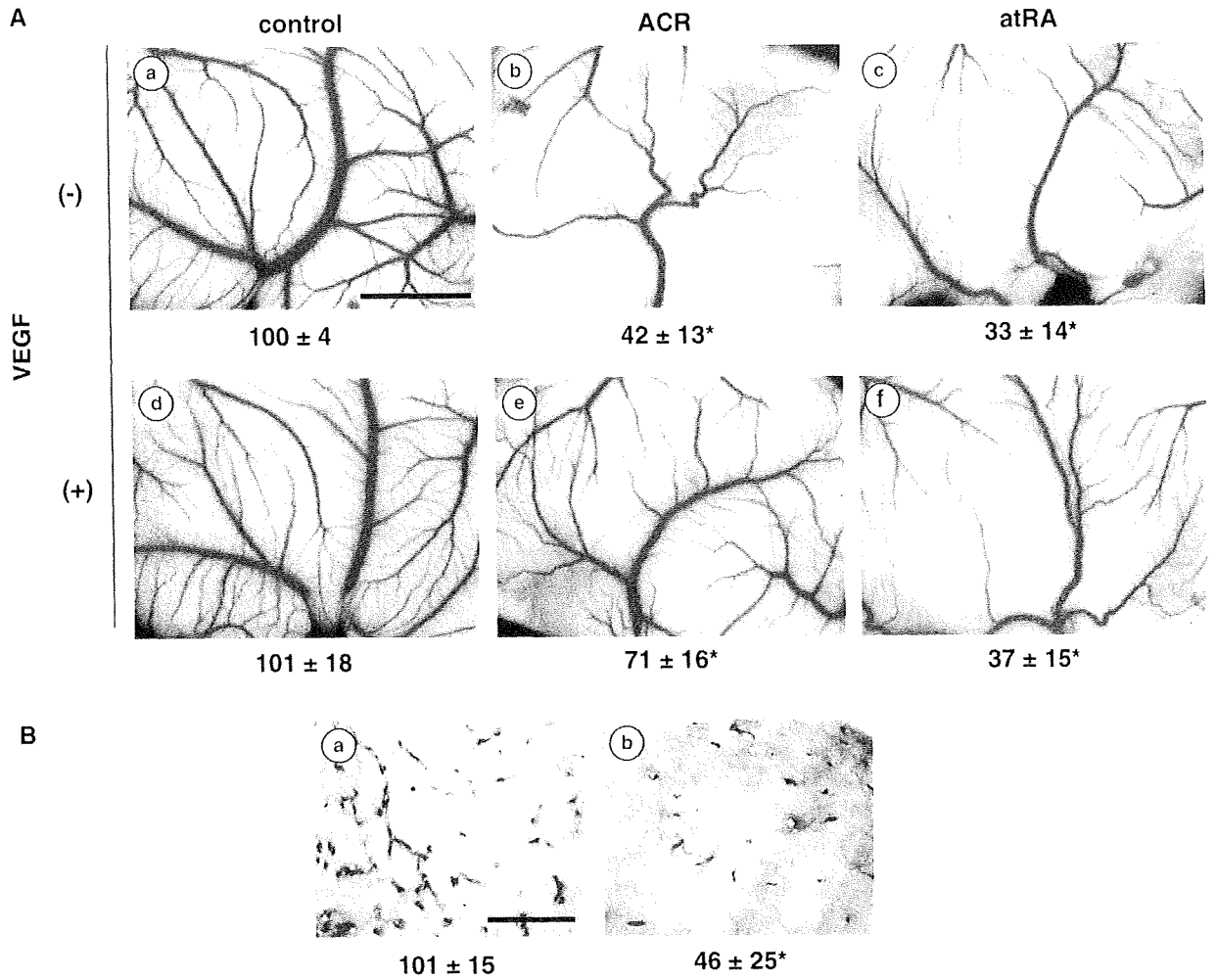

Figure 3 The antiangiogenic effect of ACR, but not of atRA, was rescued by simultaneous treatment with VEGF in CAM (**A**). The 4.5-day-old CAMs were treated with ACR and atRA for 48 h and then patterns of angiogenesis were photographed. Panel (**a**), vehicle (1% ethanol plus 1% DMSO); panel (**b**), 3 μg/egg ACR; panel (**c**), 500 ng/egg atRA; panel (**d**), vehicle plus 1 ng/egg mouse recombinant VEGF; panel (**e**), 3 μg/egg ACR plus 1 ng/egg mouse recombinant VEGF; panel (**f**) 500 ng/egg atRA plus 1 ng/egg mouse recombinant VEGF. Scale bar, 5 mm. Total numbers of branches of blood vessels were analyzed with angiogenesis-measuring software and are shown under each panel. A total of 18 eggs (6 eggs per experiment × 3 experiments) were evaluated and representative results are shown. (**B**) Matrigel plug assay: matrigel plugs containing 50 ng/ml VEGF ± 5 μM ACR were implanted into mice subcutaneously. One week later, matrigel plugs were collected and stained with hematoxylin and eosin (panels a and b). Panel **a**, VEGF alone (control); panel **b**, VEGF plus ACR. Representative data from a total of nine micrographs (3 fields × 3 mice) are presented. Scale bar, 500 μm. The number of invading cells in each micrograph was counted and the relative values are presented as percentages under each photograph. An asterisk indicates a significant difference ($P<0.05$) from the control. Panels **A** and **B** show representative results from two independent experiments, both of which gave similar results.

phosphorylation of VEGFR2 but rather increased it (compare lanes 4 with 6). Both ACR and atRA decreased the expression of VEGFR2 to about 70 and 60%, respectively, without VEGF treatment (compare lanes 1 with 2 and 3). However, this effect was not obvious in cells treated with VEGF (compare lanes 4–6). ACR did not affect the binding of VEGF to VEGFR2, nor did it affect *VEGF* mRNA levels (data not shown). On the other hand, pretreatment with ACR or atRA did not block the phosphorylation of FGFR1 but rather enhanced it (Figure 5b). Whereas ACR inhibited the phosphorylation of Ras, it did not inhibit the phosphorylation of Akt (Supplementary Figure 2). In addition, pretreatment with 5 μM ACR, but not with atRA, significantly inhibited the phosphorylation of ERK, which is induced downstream of VEGF stimuli (Figure 6a, lanes 5 and 6 in upper panel, respectively). The inhibition by ACR was inverted by the overexpression of constitutively active MAPK kinase in HUVECs (Figure 6b, lane 4 in upper panel).

Effect of ACR and atRA on HCC-Induced Angiogenesis in a Xenografted CAM Model

To confirm whether ACR and atRA have anti-HCC-induced angiogenic activity *in vivo*, we investigated the effect of ACR and atRA on HCC-induced angiogenesis in a xenografted

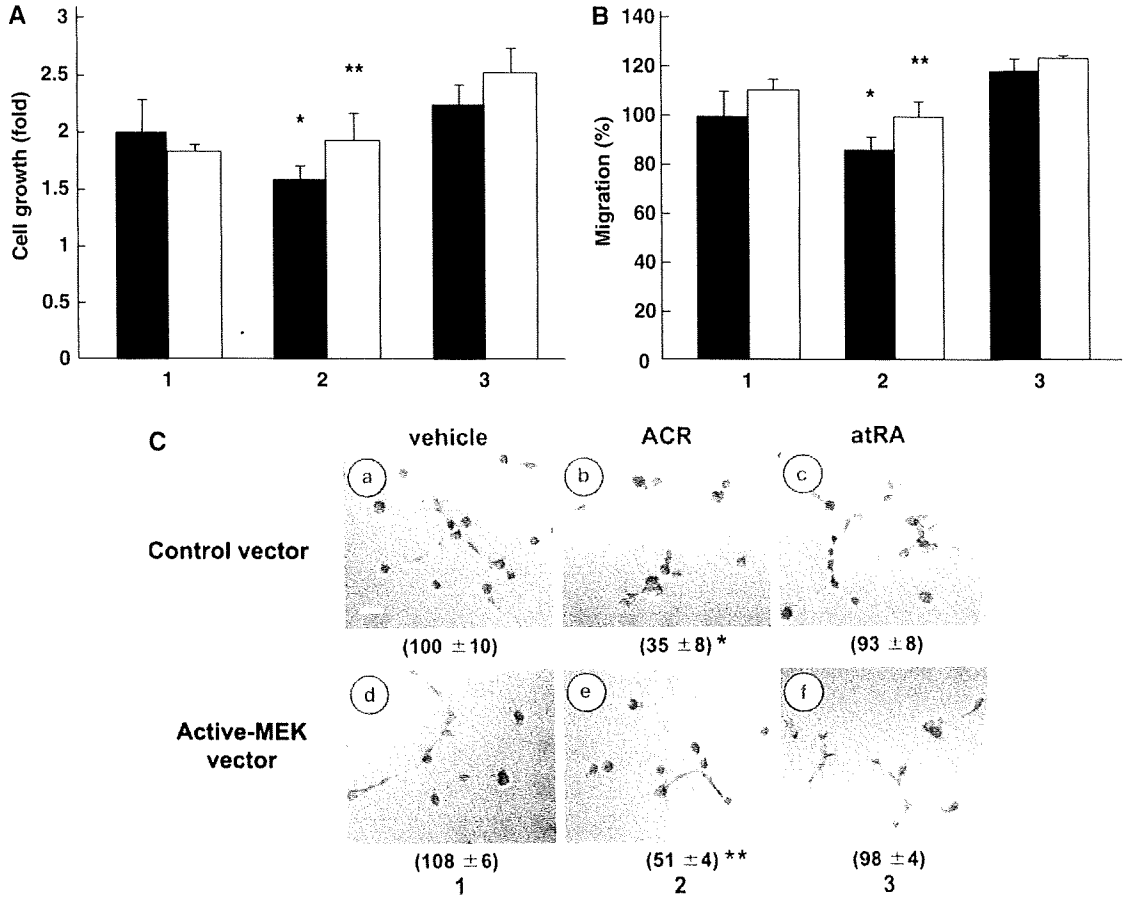

Figure 4 Effects of ACR and atRA on endothelial cell growth, migration, and tube formation. (**A**) HUVECs were transfected with a constitutively active MAPK kinase-expressing vector. After 2 days, cells (1×10^5 cells) were seeded onto 3.5-cm dishes and incubated for another 2 days. They were then incubated for 48 h in α-MEM medium containing 10% fetal calf serum, 100 ng/ml VEGF, and 5 μM ACR or atRA. Cells were counted and cell numbers are plotted as ploidy relative to values for untreated control cells at the start of incubation with ACR or atRA. Values represent means ± s.e. ($n = 2$). Lane 1, vehicle (0.1% ethanol); lane 2, ACR; lane 3, atRA. Closed columns, cells overexpressing control vector; open columns, cells overexpressing constitutively active MAPK kinase. A single asterisk indicates a significant difference ($P < 0.05$) from the control (lane 1, closed column) and double asterisks indicate a significant difference ($P < 0.05$) between samples with or without the overexpression of constitutively active MAPK kinase. (**B**) HUVECs were transfected with a constitutively active MAPK kinase-expressing vector. After 2 days, cells were wounded with a tip of pipette and incubated for 12 h in α-MEM medium containing 2.5% fetal calf serum, 100 ng/ml VEGF, and 5 μM ACR or atRA. The numbers of cells that migrated into the denuded area were counted and are plotted as percentages relative to values for untreated control cells. Values represent means ± s.e. ($n = 2$). Lane 1, vehicle (0.1% ethanol); lane 2, ACR; lane 3, atRA. Closed columns, cells overexpressing control vector; open columns, cells overexpressing constitutively active MAPK kinase. A single asterisk indicates a significant difference ($P < 0.05$) from the control (lane 1, closed column) and double asterisks indicate a significant difference ($P < 0.05$) between samples without or with the overexpression of constitutively active MAPK kinase. (**C**) HUVECs were transfected with a constitutively active MAPK kinase-expressing vector. After 2 days, cells were seeded onto polymerized matrigel at 2×10^5 cells/well. Thereafter, 100 ng/ml VEGF and 5 μM ACR or atRA were added, and incubated for 6 h. Patterns of tube formation were photographed. Scale bar, 100 μm. Panels (**a–c**), cells overexpressing control vector; panels (**d–f**), cells overexpressing constitutively active MAPK kinase. Panels (**a** and **d**), vehicle (0.1% ethanol) plus 100 ng/ml VEGF; panels (**b** and **e**), 5 μM ACR plus 100 ng/ml VEGF; panels (**c** and **f**), 5 μM atRA plus 100 ng/ml VEGF. The numbers of branches in each micrograph were counted and the relative values are presented as percentages under each photograph. A single asterisk indicates a significant difference ($P < 0.05$) from the control (panel **a** *vs* panel **b**) and double asterisks indicate a significant difference ($P < 0.05$) between samples with or without the overexpression of constitutively active MAPK kinase (panel **b** *vs* panel **e**). Panels **A–C** show representative results from two independent experiments, both of which gave similar results.

CAM model (Figure 7). Although 5 μM ACR inhibited HCC-induced angiogenesis by 37% (panel b), the same concentration of atRA did not show any inhibition at all (panel c). This result suggested that ACR, but not atRA, may prevent the recurrence of HCC in part through the inhibition of cancer angiogenesis.

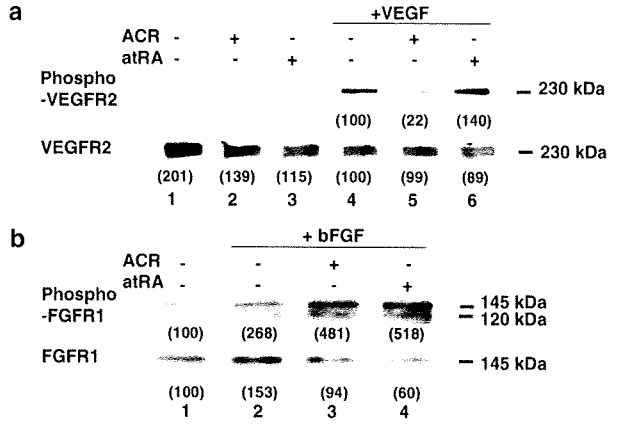

Figure 5 Effects of ACR and atRA on phosphorylation of growth factor receptors. After HUVECs had been incubated for 24 h with or without 5 μM ACR or atRA in medium containing 2.5% serum, cells were stimulated with either 100 ng/ml VEGF (panel **a**) or 50 ng/ml bFGF (panel **b**) for 5 min, and then lysed immediately. The amounts of each phosphorylated receptor (each upper bands), as well as whole amounts of each receptor (each lower bands), were assessed as described in the Materials and methods section. Panels **a** and **b** show representative results from two independent experiments, both of which gave similar results.

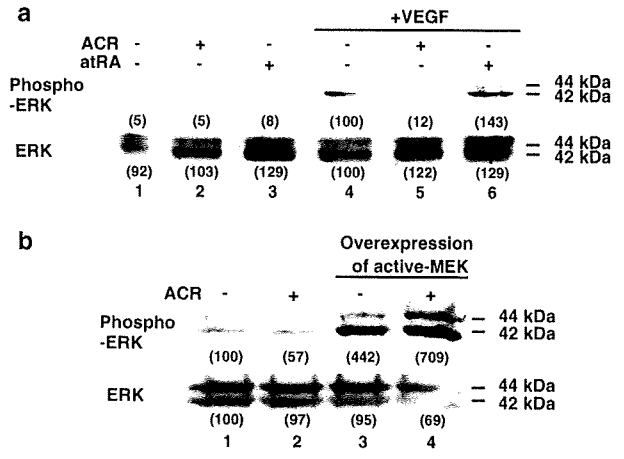

Figure 6 Effect of ACR on phosphorylation of ERK. (**a**) After HUVECs had been incubated for 24 h with or without 5 μM ACR or atRA in medium containing 2.5% serum, cells were stimulated with 100 ng/ml VEGF for 5 min and then lysed immediately. (**b**) HUVECs were transfected with a constitutively active *MEK* gene. The day after transfection, the medium was changed and cells were treated with 5 μM ACR and lysed immediately. The amounts of each phosphorylated ERK (upper bands), as well as whole amounts of ERK (lower bands), were assessed as described in the Materials and methods section.

DISCUSSION

In this paper, we have shown an antiangiogenic activity of ACR and its underlying molecular mechanism, differing from that of atRA. Although the relative antiangiogenic activity of ACR was about 10 times weaker than that of atRA at the same concentrations (Figure 1), ACR showed much stronger inhibition in endothelial cell growth, migration, and tube formation than atRA (Figure 4) because of suppression in the VEGF-MAPK pathway (Figures 5 and 6). ACR suppressed the phosphorylation of VEGFR2 (Figure 5a, lane 5). On the other hand, atRA induced the phosphorylation of VEGFR2 (Figure 5a, lane 6). This might be because of the induction of VEGF by atRA as reported previously.[17] ACR did not affect the levels of *VEGF* mRNA and the transactivation of the *VEGF* promoter (data not shown). ACR slightly inhibited the phosphorylation of VEGFR1 at 300 μM but not at all at 30 μM (Ishibashi *et al*, unpublished data). ACR (1 or 10 μM) did not inhibit other tyrosine kinases (for example, EGFR, FGFR3, FLT3, IGF1R, MET, PDGFR-α, PDGFR-β, and TRKB) (Ishibashi *et al*, unpublished data). Moreover, ACR inhibited the phosphorylation of Ras but not the phosphorylation of Akt (Supplementary Figure 2). Therefore, we speculate that ACR may selectively interfere with the phosphorylation of VEGFR2 after Ras activation, although it is not clear how ACR does this; the underlying detailed molecular mechanism(s) remain to be elucidated. ACR and atRA enhanced the phosphorylation of FGFR1 (Figure 5b, lanes 3 and 4). This result might be because of the induction of bFGF by atRA as previously reported.[18] ACR might also induce bFGF, probably through its retinoid activity.

These results suggest that suppression of the recurrence of HCC by ACR was induced in part through its antiangiogenic property by directly suppressing endothelial growth, migration, and tube formation through inhibition of the VEGFR2-MAPK axis. On the other hand, atRA inhibits angiogenesis by a disruption of vascular networks through an increased expression of Ang2 and inhibition in the Ang/Tie2 pathway.[6] Compared with atRA, ACR has 1/10–1/100 weaker 'retinoid' activities.[19] It has a 1/10 weaker action on leukemia differentiation,[20] and a 1/100 weaker carcinogenic action in transgenic mice that express the dominant-negative form of retinoic acid receptor.[21,22] On the other hand, accumulating evidence shows that ACR, but not atRA, has apoptosis-inducing activity in HCC cells, as well as in smooth muscle cells and vascular neointima.[23,24] We found that ACR acts as either a kinase inhibitor or a phosphatase stimulator and prevents hyperphosphorylation of RXR,[9] and now VEGFR2. In this context, we speculate that ACR resembles geranylgeraniol in terms of its isoprenoid-like structure, which has been implicated in the modulation of many phosphorylation/dephosphorylation signaling.[25,26]

Hepatocellular carcinoma is a major cause of cancer mortality worldwide, especially in Southeast Asia and in sub-Saharan Africa.[27] The development of HCC is frequently associated with a chronic inflammation of the liver induced by persistent infection with hepatitis B virus or hepatitis C virus. The annual incidence rises to ~20–25% in cirrhotic patients who have undergone a potentially curative removal of primary HCC in Japan; the recurrence rate at 5 years after the curative treatment may exceed 70%. This high recurrence rate is not because of local recurrence or metastasis from the original lesion, but rather from a second primary lesion.[19]

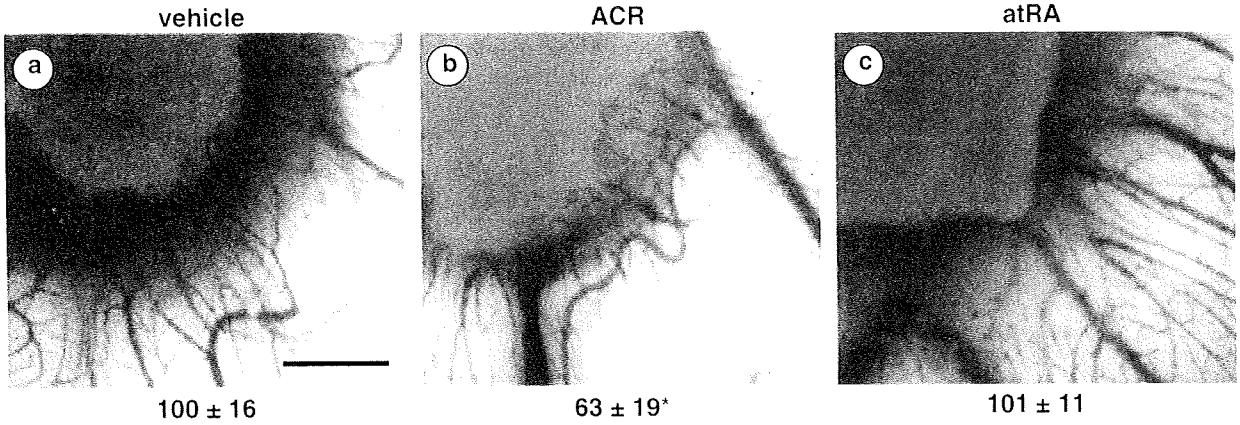

Figure 7 Effect of ACR on HCC-induced angiogenesis on CAM. HepG2 cell suspensions with or without 5 μM ACR or atRA were delivered at 4×10^5 cells per embryo onto the top of CAM on day 8 using a gelatin sponge implant. After a further 4-day incubation, a fat emulsion was injected into the chorioallantois, so that the vascular networks stood out against the white background of the lipid, and patterns of angiogenesis toward the implant were photographed. Panel (**a**), vehicle (1% EtOH); panel (**b**), 5 μM ACR; panel (**c**), 5 μM atRA. Scale bar, 1 mm. Total numbers of branches of blood vessels were counted and the relative values are presented as percentages under each photograph. An asterisk indicates a significant difference ($P<0.05$) from the control. This result shows the representative result from two independent experiments, both of which gave similar results.

In HCC tissues, RXR-α is constitutively phosphorylated by the activation of MAPK, resulting in a loss of its function and accumulation of inactive RXR-αs inside cells as dominant-negative inhibitors.[9,10] Therefore, phosphorylation of RXR-α causes a reduction in transactivation through a RAR/RXR complex.[9,28] ACR inhibits the phosphorylation of RXR-α and restores the function of RXR-α, and thereby transactivation through the RAR/RXR complex with endogenous retinoic acid. Retinoids are thought to activate the transcription of cell cycle inhibitor $p21^{CIP1}$ by RAR[29] and by apoptosis-inducer tissue transglutaminase in HCC.[19] However, 5 μM ACR hardly induces endothelial cell death (Figure 4A) and expression of $p21^{CIP1}$ mRNA levels in endothelial cells (data not shown). We found that phosphorylation of RAR/RXR was associated with the growth of endothelial cells and that ACR inhibited this phosphorylation (Supplementary Figure 3). As this phosphorylation of RAR/RXR coincided with the activation of VEGFR2 and Ras and as we had already found that RAR/RXR phosphorylation was induced by the overexpression of active MEK in cancer cells,[10] we speculate that phosphorylation of RAR/RXR would occur downstream of the VEGF/VEGFR axis in growing endothelial cells.

Acyclic retinoid suppressed both angiogenesis and HCC-induced angiogenesis in a xenografted CAM model (Figure 1, panels b–d and Figure 7, panel b, respectively). In this model, ACR did not affect the preexisting blood vessels on CAM. These results suggest that ACR did not affect the mature blood vessel and only affected neovasculature formation, including both normal angiogenesis and tumor angiogenesis. On the other hand, atRA suppressed angiogenesis but failed to suppress the tumor angiogenesis on CAM (Figures 1 and 7, panels e–g and panel c, respectively), suggesting that atRA inhibits angiogenesis in the embryonic stage, but not tumor-induced angiogenesis, and addressing the superiority of ACR as a promising antitumor angiogenesis agent. The dose of ACR used in this experiment (5 μM) is higher than the maximal blood concentration of ACR in clinical use (1 μM) (Ishibashi *et al*, unpublished data). However, we believe that liver tissue has higher doses of ACR than does the blood level because of the accumulation of ACR in the liver. These results suggest that one of the mechanisms of ACR action to prevent recurrence of HCC is its antiangiogenic activity.

Supplementary Information accompanies the paper on the Laboratory Investigation website (http://www.laboratoryinvestigation.org)

ACKNOWLEDGEMENTS
The authors thank Dr NG Ahn (University of Colorado, CO) for providing the constitutively active MAPK kinase vector. This study was supported in part by grants from the Chemical Genomics Research Project from RIKEN (to SK) and Grant-in-Aids from the Ministry of Education, Science, Sports, and Culture (17015016, HM).

DISCLOSURE/CONFLICT OF INTEREST
The authors declare no conflict of interest.

1. Mazitschek R, Giannis A. Inhibitors of angiogenesis and cancer-related receptor tyrosine kinase. Curr Opin Chem Biol 2004;8:432–441.
2. Ferrara N, Kerbel R. Angiogenesis as a therapeutic target. Nature 2005;438:967–974.
3. Chambon P. A decade of molecular biology of retinoic acid receptors. FASEB J 1996;10:940–954.
4. Obora A, Shiratori Y, Okuno M, *et al.* Synergistic induction of apoptosis by acyclic retinoid and interferon-β in human hepatocellular carcinoma cells. Hepatology 2002;36:1115–1124.
5. Altucci L, Leibowitz MD, Ogilvie KM, *et al.* RAR and RXR modulation in cancer and metabolic disease. Nat Rev Drug Discov 2007;6:793–810.
6. Suzuki Y, Komi Y, Ashino H, *et al.* Retinoic acid controls blood vessel formation by modulating endothelial and mural cell interaction via suppression of Tie2 signaling in vascular progenitor cells. Blood 2004;104:166–169.